



The structure of *Medicago truncatula* δ^1 -pyrroline-5-carboxylate reductase provides new insights into regulation of proline biosynthesis in plants

Milosz Ruszkowski^{1*}, Boguslaw Nocek², Giuseppe Forlani³ and Zbigniew Dauter¹

¹ Synchrotron Radiation Research Section, Macromolecular Crystallography Laboratory, National Cancer Institute, Argonne, IL, USA, ² Biosciences Division, Argonne National Laboratory, The Structural Biology Center, Argonne, IL, USA, ³ Department of Life Science and Biotechnology, University of Ferrara, Ferrara, Italy

OPEN ACCESS

Edited by:

Shabir Hussain Wani,
SKUAST-Kashmir, India

Reviewed by:

Taras P. Pasternak,
Albert-Ludwigs-Universität Freiburg,
Germany

Vinay Kumar,
Modern College of Arts, Science and
Commerce, India

*Correspondence:

Milosz Ruszkowski
mruszkowski@anl.gov

Specialty section:

This article was submitted to
Plant Biotechnology,
a section of the journal
Frontiers in Plant Science

Received: 31 August 2015

Accepted: 01 October 2015

Published: 30 October 2015

Citation:

Ruszkowski M, Nocek B, Forlani G
and Dauter Z (2015) The structure of
Medicago truncatula
 δ^1 -pyrroline-5-carboxylate reductase
provides new insights into regulation
of proline biosynthesis in plants.
Front. Plant Sci. 6:869.
doi: 10.3389/fpls.2015.00869

The two pathways for proline biosynthesis in higher plants share the last step, the conversion of δ^1 -pyrroline-5-carboxylate (P5C) to L-proline, which is catalyzed by P5C reductase (P5CR, EC 1.5.1.2) with the use of NAD(P)H as a coenzyme. There is increasing amount of evidence to suggest a complex regulation of P5CR activity at the post-translational level, yet the molecular basis of these mechanisms is unknown. Here we report the three-dimensional structure of the P5CR enzyme from the model legume *Medicago truncatula* (*Mt*). The crystal structures of unliganded *Mt*P5CR decamer, and its complexes with the products NAD⁺, NADP⁺, and L-proline were refined using x-ray diffraction data (at 1.7, 1.85, 1.95, and 2.1 Å resolution, respectively). Based on the presented structural data, the coenzyme preference for NADPH over NADH was explained, and NADPH is suggested to be the only coenzyme used by *Mt*P5CR *in vivo*. Furthermore, the insensitivity of *Mt*P5CR to feed-back inhibition by proline, revealed by enzymatic analysis, was correlated with structural features. Additionally, a mechanism for the modulation of enzyme activity by chloride anions is discussed, as well as the rationale for the possible development of effective enzyme inhibitors.

Keywords: protein structure, decamer, coenzyme preference, salt stress, abiotic stress, P5C reductase, P5CR

INTRODUCTION

In plant cells the function of proline goes much further than being a building block for proteins (Szabados and Savouré, 2010). Many studies have shown that free proline can trigger signal transduction pathways associated with different stress responses. The signaling function of proline was first observed in bacteria and was related to osmotic stress (Csonka, 1988; Csonka et al., 1988; Csonka and Hanson, 1991). Later on, proline was also reported to be a key player in plant adaptation to adverse environmental conditions (Verslues and Sharma, 2010), such as high salinity (Yoshida et al., 1995), drought (Choudhary et al., 2005), abnormal doses of UV radiation (Saradhi et al., 1995), exposure to heavy metals (Schat et al., 1997), reactive oxygen species (Yang et al., 2009), and pathogens (Fabro et al., 2004; Haudecoeur et al., 2009). Interestingly, it was recently reported that free proline can also regulate development, flowering and reproduction (Mattioli et al., 2008, 2009; Funck et al., 2012).

In higher plants, proline can be synthesized *via* two main pathways, one starting from glutamate (Smith et al., 1980; Székely et al., 2008) and the other from ornithine (Abdelal, 1979; da Rocha et al., 2012). The first route, localized either in the cytoplasm or in the chloroplast (Lehmann et al., 2010), involves phosphorylation of glutamate to γ -glutamyl phosphate and its reduction to glutamate γ -semialdehyde (GSA), which undergoes spontaneous, non-enzymatic cyclization to δ^1 -pyrroline-5-carboxylate (P5C). The two enzymatic steps are catalyzed by a bifunctional P5C synthetase (P5CS; EC 2.7.2.11/1.2.1.41). In the second pathway, ornithine is directly transformed into GSA/P5C by a mitochondrial ornithine δ -aminotransferase (OAT; EC 2.6.1.13; Winter et al., 2015). The pathway preference appears to depend on nitrogen availability, being the ornithine route preferred under nitrogen-rich conditions (Delauney and Verma, 1993; da Rocha et al., 2012). Both routes converge at the generation of P5C, which in the final step (**Figure 1**) is reduced to L-proline by P5C reductase (P5CR, EC 1.5.1.2). This means that P5CR is always required for proline biosynthesis. Consistently, null mutations in *p5cr* genes are embryo lethal (Funck et al., 2012), and targeting specific inhibitors of P5CRs is of great interest as a solution for weed control (Forlani et al., 2007, 2013).

Salt and drought stress-induced proline synthesis plays a main role in legume plants, where both the ornithine (through enhanced transcription of *OAT*) and the glutamate pathways (*P5CS isozyme 2*) contribute to proline accumulation (Armengaud et al., 2004). Under osmotic stress conditions, the efficiency of establishment of the *Rhizobium*-legume symbiosis and the rate of nitrogen fixation are dramatically affected, reducing crop yield, and soil-enriching capacity (Coba de la Peña et al., 2003). Interestingly, high proline concentrations have been found in fava bean symbiosomes, which significantly increased in response to treatments with NaCl (Trinchant et al., 1998). Stress-induced proline accumulation was higher in the peribacteroid space, whereas very low rates of proline uptake by bacteroids were found, suggesting a role for proline as osmoticum rather than energy source for bacterial symbionts (Trinchant et al., 1998). Consistently, proline overaccumulating transgenic *Medicago truncatula* plants displayed nitrogen-fixing activity with enhanced tolerance to osmotic stress (Verdoy et al., 2006). Moreover, higher P5CR activity in ureide-exporting than in amide-exporting nodules led to hypothesize that NADP⁺ production, deriving from the reduction of P5C, may be also functional to fuel the oxidative pentose phosphate pathway (OPPP), which is required for the synthesis of ureides (Kohl et al., 1990). The complexity of proline metabolism and its regulation

in legume plants is witnessed by the discovery in *M. truncatula* of a third gene coding for a P5CS isozyme, which has been shown to play a predominant role in stress-induced proline accumulation during symbiotic nitrogen fixation (Kim and Nam, 2013).

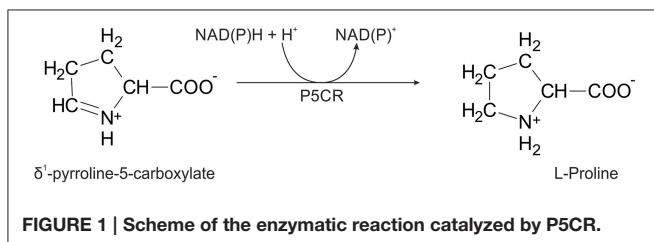
While the three-dimensional structures of human and some bacterial P5CR orthologs have been determined, to date high-resolution crystal structures of plant P5CRs have been absent. This hampered the possibility of deeper understanding of enzyme features and post-translational regulative mechanisms. Indeed, plant P5CRs have been recently found to be subjected to a complex pattern of regulation by coenzyme availability, product inhibition and ion effects (Giberti et al., 2014; Forlani et al., 2015a), supporting a so far underestimated role of P5CR in controlling stress-induced proline accumulation. These mechanisms may allow the plant enzyme to respond to wide fluctuations of P5C synthesis by either P5CS isozymes or OAT without the need of a transcriptional control. However, the molecular basis of the pyridine nucleotide coenzyme preference, i.e., the P5CR protein fragment responsible for NADH/NADPH discrimination, has not yet been determined. Also, the residues connected to the lack of feed-back inhibition by proline and those involved in inhibition or stimulation of the P5CR activity by chloride anions have not yet been described.

Here we report the high-resolution crystal structure of P5CR from *M. truncatula* (*Mt*), a model legume plant. For these studies, *Mt*P5CR was expressed heterologously in *Escherichia coli* cells, purified and characterized. Four crystal structures were then solved: unliganded *Mt*P5CR, its complexes with NAD⁺, NADP⁺, and L-proline. The structural data were related to the enzymatic properties, with special attention to the coenzyme preference (NADPH vs. NADH) and modulation of *Mt*P5CR activity by chloride anions. Additionally, because a 3-(*N*-morpholino)propansulfonate (MOPS) molecule was found within the active center of the *Mt*P5CR structure, the inhibitory properties of some sulfonates have been investigated, allowing us to propose 2-[4-(2-hydroxyethyl)piperazin-1-yl]ethanesulfonic acid (HEPES) as a putative starting molecule in the design of new P5CR inhibitors.

MATERIALS AND METHODS

Cloning, Overexpression, and Purification of *Mt*P5CR

Total RNA was isolated from *M. truncatula* leaves using the RNeasy Plant Mini Kit (Qiagen). SuperScript II reverse transcriptase (Life Technologies) with oligo dT (15 and 18) primers was utilized to obtain the complementary DNA (cDNA). The cDNA was used as a template to acquire the *Mt*P5CR gene sequence by polymerase chain reaction. The primers used (Forward: TACTTCCAATCCAATGCCATGGAAATCATTTCCGATCCCCGC, Reverse: TTATCCACTTCC AATGTTATCAGGAAAGCTCTTGGCTGCGTTTA) allowed for incorporating the gene into the pMCSG68 vector (Midwest Center for Structural Genomics Eschenfeldt et al., 2013) by



ligase-independent cloning (Kim et al., 2011). The pMCSG68 vector introduces a His₆-tag followed by the tobacco etch virus (TEV) protease cleavage site at the N-terminus of the expressed protein. The correctness of the insert was confirmed by DNA sequencing.

Overexpression was carried out in BL21 Gold *E. coli* cells (Agilent Technologies). The bacteria were cultured with shaking at 210 rpm in LB medium supplemented with 150 µg mL⁻¹ ampicillin at 37°C until the OD₆₀₀ reached 1.0. The temperature was lowered to 18°C and isopropyl-β-D-thiogalactopyranoside (IPTG) was added to a final concentration of 0.5 mM. The culture was grown for 18 h and then centrifuged at 3500 × *g* for 10 min at 4°C. A cell pellet from 1 L culture was resuspended in 35 mL of binding buffer (50 mM Tris-HCl pH 8.0, 500 mM NaCl, 20 mM imidazole, 1 mM tris(2-carboxyethyl)phosphine [TCEP]) and stored at -80°C. The samples were thawed and the cells were disrupted by sonication using four bursts for a total duration of 4 min, with 20 s intervals for cooling. Cell debris was pelleted by centrifugation at 25,000 × *g* for 30 min at 4°C. The supernatant was applied to a column packed with 6 mL of HisTrap HP resin (GE Healthcare), connected to a VacMan manifold (Promega) and the chromatographic process was accelerated with a vacuum pump. After binding, the column was washed with five 40-mL volumes of the binding buffer and the His₆-tagged MtP5CR was eluted with 20 mL of elution buffer (50 mM Tris-HCl pH 8.0, 500 mM NaCl, 300 mM imidazole, 1 mM TCEP). The His₆-tag was cleaved with TEV protease (final concentration 0.1 mg mL⁻¹) and the excess imidazole was removed by dialysis (overnight at 4°C) simultaneously. The solution was mixed with HisTrap HP resin to eliminate the cleaved His₆-tag and the His₆-tagged TEV protease. The flow-through was collected, concentrated to 4 mL and applied onto a HiLoad Superdex 200 16/60 column (GE Healthcare) equilibrated with a buffer composed of 50 mM Tris-HCl pH 8.0, 200 mM NaCl, and 1 mM TCEP. Size exclusion chromatography yielded a homogenous protein fraction.

Crystallization and Data Collection

The MtP5CR solution was concentrated using Amicon concentrators (Millipore) to 22 mg mL⁻¹, as determined by measuring the absorbance at 280 nm on the basis of an extinction coefficient of 17,000 M⁻¹ cm⁻¹. Crystallization screening was performed using a robotic sitting drop vapor diffusion setup (Mosquito). The most promising hits were optimized manually in hanging drops. The final conditions were obtained from the Morpheus screen (Molecular Dimensions) A7 solution (100 mM HEPES/MOPS buffer pH 7.5, 10% polyethylene glycol 4000, 20% glycerol, 30 mM MgCl₂, 30 mM CaCl₂). The crystallization drop was composed of 4 µL of protein and 2 µL of the reservoir solution. Crystals with ~0.5 × 0.5 × 0.5 mm dimensions appeared after 5 days at 19°C. Aiming at obtaining MtP5CR/NAD⁺ and MtP5CR/NADP⁺ complexes, the protein was incubated with either of the two coenzymes (at a 4 mM final concentration) for 10 min at room temperature and centrifuged at 17,000 × *g* prior to the crystallization setup. The analogous cocrystallization failed while obtaining the structure of the L-proline complex, as

determined by inspection of the resulting electron density maps. Therefore, 0.1 µL of 1 M L-proline, dissolved in the reservoir solution, was added to the drop containing grown crystals of the unliganded MtP5CR. The crystallization conditions provided sufficient cryo-protection and the crystals were harvested and flash frozen in liquid nitrogen.

The diffraction data collected at beamline 19-ID at Advanced Photon Source, Argonne, USA (Rosenbaum et al., 2006). The diffraction images for the unliganded, NAD- and NADP-bound MtP5CR were processed with XDS (Kabsch, 2010), while the HKL3000 package (Minor et al., 2006) was utilized in the case of the MtP5CR/L-proline complex. The data collection and processing statistics are summarized in **Table 1**. Diffraction data at 1.7196 Å wavelength were collected at beamline 19-BM. To increase the multiplicity of measurements, four datasets, each differing only by 10-pixels shifts of the detector, were processed and scaled with XDS.

Determination and Refinement of the Crystal Structures

The crystal structure of MtP5CR was determined by molecular replacement using the PHASER program (McCoy et al., 2007). A decamer created from the closest homolog with the available crystal structure, namely the human P5CR with 34% identity (PDB ID: 2izz), was used as a search probe. Automatic model building was carried out with the online version of ARP/wARP (Langer et al., 2008). The atomic coordinates were placed inside the unit cell using the ACHESYM server (Kowiel et al., 2014). The protein chain from the unliganded MtP5CR (the structure without a bound coenzyme or L-proline) was used as the initial model for refinement of the other complexes, which are all isomorphous. COOT (Emsley et al., 2010) was used for manual fitting in the electron density maps between rounds of model refinement using Refmac (Murshudov et al., 2011) with local non-crystallographic symmetry (NCS) restraints. Additional, secondary structure restraints, generated with ProSMART (Nicholls et al., 2014), were applied for poorly defined regions of the G chains of the unliganded MtP5CR and the complex with L-proline. Translation/Libration/Screw (TLS) parameters (Winn et al., 2001) were refined for twenty groups in each of the four structures. More precisely, each protein chain was divided into two TLS groups corresponding to the two distinctive domains: the NAD(P)-binding domain (N-terminus:Asp169) and the dimerization domain (Lys170:C-terminus). Riding hydrogen atoms for the protein chain were included in the refinement. The refinement statistics are listed in **Table 1**.

Biochemical Analysis

The physiological, forward reaction of P5CR was measured at 35°C following the P5C-dependent oxidation of NAD(P)H. Unless otherwise specified, the assay mixture contained 50 mM Tris-HCl buffer pH 7.5, 1 mM NADH or 0.5 mM NADPH, and 2 mM DL-P5C (equivalent to 1 mM L-P5C; Williams and Frank, 1975) in the final volume of 0.2 mL. DL-P5C was synthesized by the periodate oxidation of δ-allo-hydroxylysine (Sigma H0377) and purified by cation-exchange chromatography, as described

TABLE 1 | Data-collection and refinement statistics; values in parentheses correspond to the highest resolution shell.

| MtP5CR: | Unliganded | NAD ⁺ | NADP ⁺ | L-Proline | Anomalous |
|---------------------------------------------------------|--------------------------|--------------------------|--------------------------|------------------------|--------------------------|
| DATA COLLECTION | | | | | |
| Wavelength (Å) | 0.9790 | 0.9790 | 0.9786 | 0.9786 | 1.7196 |
| Temperature (K) | 100 | 100 | 100 | 100 | 100 |
| Space group | <i>P</i> 1 | <i>P</i> 1 | <i>P</i> 1 | <i>P</i> 1 | <i>P</i> 1 |
| Unit cell parameters | | | | | |
| <i>a</i> , <i>b</i> , <i>c</i> (Å) | 86.8, 100.6, 101.2 | 87.5, 100.8, 101.6 | 87.2, 100.3, 100.8 | 87.2, 101.1, 101.5 | 87.2, 101.2, 101.9 |
| α , β , γ (°) | 67.9, 85.3, 89.3 | 67.5, 85.9, 89.8 | 68.1, 85.8, 89.3 | 67.4, 85.4, 89.6 | 67.7, 85.6, 89.5 |
| Oscillation range (°) | 0.5 | 0.5 | 1 | 0.5 | 1 |
| No. of images | 680 | 680 | 300 | 500 | 4 × 240 |
| Resolution (Å) | 40.0-1.70 (1.74-1.70) | 40.0-1.85 (1.90-1.85) | 40.0-1.95 (2.06-1.95) | 40-2.10 (2.14-2.10) | 40.0-2.50 (2.57-2.50) |
| Reflections collected/Unique | 1383055/338502 | 978057/266309 | 732206/225659 | 481562/183949 | 1097686/208539 |
| Completeness (%) | 97.2 (95.6) | 97.4 (96.2) | 96.9 (92.5) | 97.7 (96.7) | 93.8 (83.8) |
| Multiplicity | 4.1 (3.4) | 3.7 (3.7) | 3.2 (3.2) | 2.6 (2.6) | 5.3 (4.9) |
| <i>R</i> _{meas} ^a (%) | 5.0 (79.9) | 5.3 (75.0) | 13.6 (87.6) | 8.6 (60.8) | 4.2 (22.9) |
| < <i>I</i> / σ (<i>I</i>)> | 15.2 (1.9) | 17.7 (2.0) | 10.7 (2.0) | 13.3 (1.9) | 33.4 (7.3) |
| REFINEMENT | | | | | |
| <i>R</i> _{free} reflections | 2708 | 2131 | 2257 | 1941 | |
| No. of atoms (non-H) | 21823 | 22411 | 22670 | 20686 | |
| Protein | 20277 | 20161 | 20086 | 19911 | |
| Ligands | 75 | 580 | 620 | 80 | |
| Solvent | 1471 | 1670 | 1964 | 695 | |
| <i>R</i> _{work} / <i>R</i> _{free} (%) | 16.0/18.0 | 15.5/17.7 | 15.5/17.8 | 18.0/19.7 | |
| Mean atomic displacement parameter (Å ²) | 52.7 | 41.4 | 31.3 | 74.0 | |
| RMSD from ideal geometry | | | | | |
| Bond lengths (Å) | 0.020 | 0.021 | 0.019 | 0.017 | |
| Bond angles (°) | 1.9 | 1.9 | 1.8 | 1.6 | |
| Ramachandran statistics (%) | | | | | |
| Favored | 99.5 | 99.1 | 99.0 | 99.3 | |
| ALLOWED | 0.5 | 0.9 | 1.0 | 0.7 | |
| Outliers | 0.0 | 0.0 | 0.0 | 0.0 | |
| PDB code | 5bse | 5bsf | 5bsg | 5bsh | |

^a*R*_{meas} = redundancy independent *R*-factor (Diederichs and Karplus, 1997).

previously (Forlani et al., 1997). P5C solution was neutralized with 1 M Tris base (pH ~11) immediately before use. A limiting amount of MtP5CR (7 ng of the purified protein in 10 μ L buffer, 1.3 nM final concentration) was added to the pre-warmed mixture. The decrease of absorbance at 340 nm was recorded with 30 s intervals for 5 min through an optical path of 0.5 cm. Activity was calculated from the initial linear rate on the assumption of a molar extinction coefficient for NAD(P)H of 6220 M⁻¹ cm⁻¹. Linear regression analysis was computed with Prism 6 (version 6.03, GraphPad Software, Inc., USA).

To calculate apparent Michaelis-Menten constants (*K*_{M(app)}), invariable substrates were fixed at the same levels as in the standard assay. The concentration of L-P5C ranged from 50 to 400 μ M with NADH as the electron donor, and from 25 to 200 μ M with NADPH as the electron donor. The concentrations of NADH and NADPH ranged from 200 to 800 μ M and from 50 to 200 μ M, respectively. When evaluating the effect

of NaCl, the L-P5C concentration was reduced to 200 μ M to minimize the carryover of chloride anions. All assays were performed in triplicate. *K*_M and *V*_{max} values, as well as the concentrations causing 50% inhibition (IC₅₀) of P5CR activity, *K*_I values and their confidence intervals were estimated by non-linear regression analysis using Prism 6. Catalytic constants were calculated from *V*_{max} values, taking into account a homodecameric composition of the native holoenzyme, each monomer having a molecular mass of 28.5 kDa.

Other Software Used

Molecular figures were created with UCSF *Chimera* (Pettersen et al., 2004). RMSDs were calculated with the same program for C α atoms within 3 Å radius. Assignment of secondary structure elements was based on the DSSP algorithm (Kabsch and Sander, 1983) and PDBsum web server (de Beer et al., 2014). Ramachandran plots were calculated in *Rampage* (Lovell et al., 2003).

RESULTS

Cloning of the Gene Coding for Pyrroline-5-Carboxylate Reductase in *M. truncatula*

According to the UniProt knowledgebase (UniProt Consortium, 2015), in the legume *M. truncatula* there should be two P5CR isoforms (*MtP5CR_1* and *MtP5CR_2*). However, they have a nearly identical sequence, except for a 29 amino acid insert in *MtP5CR_2* between Leu83 and Leu84 of *MtP5CR_1* (Figure 2). This insert contains an unusually high number of hydrophobic residues, and a BLAST (Altschul et al., 1997) search revealed no P5CRs with similar inserts in other species. Moreover, a recent and comprehensive analysis of plant P5CRs from a phylogenetic perspective failed to find support for the occurrence of two genes in this species (Forlani et al., 2015b). In another legume, *Glycine max*, two genes are indeed present that show 94% identity, suggesting recent duplication, but none of them contains an insert similar to that of *MtP5CR_2*. Therefore, *MtP5CR_1* was cloned as the genuine gene coding for P5CR in *M. truncatula*. The sequence conservation between *MtP5CR* and its orthologs (Figure 2) is high among plants, and exceptionally high among legumes, equaling (identity/similarity in %) 73/87 for *Arabidopsis thaliana* (*At*), 63/77 for *Oryza sativa* (*Os*), 92/95 for *Pisum sativum* (*Ps*), 85/93 for *Glycine max* (*Gm*), 34/51 for *Homo sapiens* (*Hs*), 30/50 for *Streptococcus pyogenes* (*Sp*), and 29/46 for *Neisseria meningitidis* (*Nm*).

MtP5CR Shows a Complex Pattern of Activity Regulation by Substrates, Products, and Salts

MtP5CR kinetic parameters were determined. Results are summarized in Table 2. Maximal activity was obtained with NADH as the electron donor, corresponding to a catalytic constant of almost 3000 catalytic events s^{-1} per monomer. When NADPH was used as the coenzyme instead of NADH, a remarkably lower V_{max} value was obtained. However, the $K_{M(app)}$ found for P5C is 12-fold lower when NADPH is used as the coenzyme. The corresponding constants for either coenzyme showed a similar trend, with apparent K_M values of 39 and 468 μM for NADPH and NADH, respectively. Fully saturating conditions for NADH were not obtained, even at the highest concentration used (1 mM).

When the activity of *MtP5CR* (NADH vs. NADPH-dependent reaction) was measured in the presence of increasing concentrations of $NADP^+$ or NAD^+ , an inhibitory effect was found only in the case of $NADP^+$ (Figure 3). NAD^+ was ineffective in the range of concentrations tested (up to 10 mM, data not shown). Interestingly, the inhibition caused by $NADP^+$ was drastically stronger when NADH was the electron donor. With equimolar levels of the oxidized and the reduced forms, the NADH-dependent activity was inhibited by 80%, whereas the NADPH-dependent reaction rate was reduced only by 20%. Quite unexpectedly, and contrary to what previously found for the enzyme from *A. thaliana* and rice (Giberti et al., 2014; Forlani et al., 2015a), proline in the range from 1

to 100 mM inhibited neither the NADH-dependent nor the NADPH-dependent activity of *MtP5CR*.

When the impact of chloride ions on enzyme activity was evaluated, results were contrasting depending on the concentration. In the range of 20–200 mM, a progressive stimulation was observed. Over this threshold, the results were opposite, as the activity was steadily reduced (data not shown). Also in this case, the effect was different if NADH or NADPH was the coenzyme, with IC_{50} values of 485 ± 21 or 704 ± 7 mM, respectively. However, with NaCl it is impossible to distinguish the effect of Cl^- anions from that of Na^+ cations. Therefore, the experiment was repeated by adding the two ions separately, as Na-Tricine or Tris-HCl. Preliminary trials ruled out the possibility that tricine anions or Tris cations significantly influenced enzyme activity (data not shown). The results, shown in Figure 4, clearly pointed at chlorides as the main effectors. Once again, the effect differed depending on the coenzyme used. With NADH, a 1.8-fold stimulation of enzyme activity was found with the addition of 100 mM Cl^- to the reaction mixture, then activity was progressively inhibited, with an IC_{50} value of 161 ± 6 mM. Under the same conditions, but with NADPH instead of NADH, P5CR activity was stimulated seven-fold, and the subsequent inhibition took place at higher concentrations, with an IC_{50} value of 451 ± 15 mM. The addition of equimolar levels of Na^+ had, on the contrary, minor effects and, in the case of NADH, only a progressive inhibition of enzyme activity was evident.

The *MtP5CR* Protein is a Decamer of Five Dimers with Higher Structural Similarity with the Bacterial Orthologs than with the Human Enzyme

Crystals of unliganded *MtP5CR* and its complexes with the products NAD^+ , $NADP^+$ and L-proline were obtained, and their structures were refined using high-resolution diffraction data (Table 1). In this paper, the term “unliganded” refers to the structure without a coenzyme or L-proline, despite the fact that it actually contains non-protein and non-solvent ligands. The protein crystallized in the *P1* space group, with one decamer (chains A–J) as the asymmetric unit. The decameric quaternary structure in the crystal lattice was in agreement with the size-exclusion elution profile of *MtP5CR* (data not shown). Crystals of *MtP5CR* contained about 57% solvent. Two to six (chain-dependent) N-terminal residues were not defined in the electron density maps and are not present in the deposited coordinate files. On the other hand, each C-terminus was modeled completely. In the complex with L-proline (2.1 Å resolution), the protein chain for residues 43–46 (in chains C and D) and 43–49 (chain G) was disordered. The structures with a bound coenzyme, despite having poorer data resolution (1.85 Å with NAD^+ and 1.95 Å with $NADP^+$) than the unliganded structure (1.7 Å), had lower average atomic displacement parameters, and allowed for tracing more water molecules (Table 1).

The donut-shaped decamer of *MtP5CR* can be described as a pentamer of symmetric, bean-like dimers (Figure 5) that are related to each other by a five-fold NCS axis. The molecules

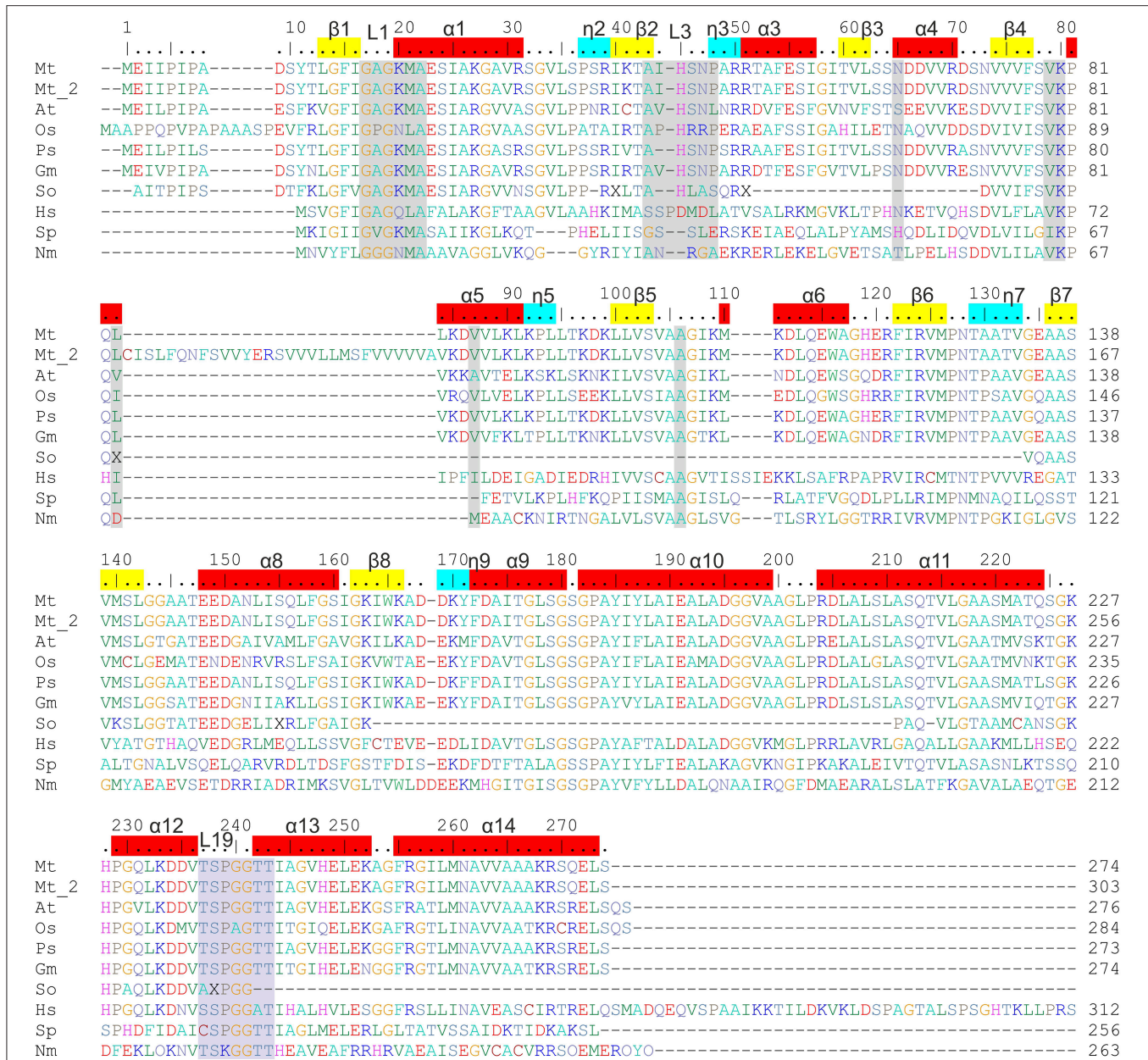


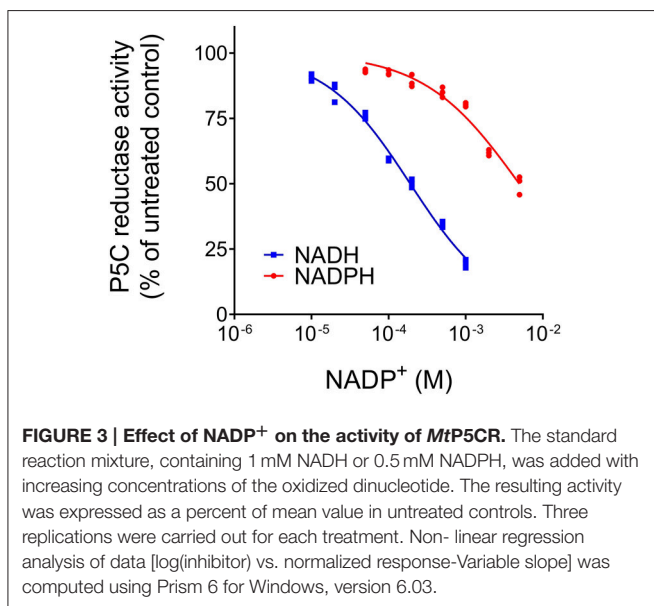
FIGURE 2 | Sequence alignment of P5CRs from various sources. The following organisms are listed and square brackets indicate UniProt accession numbers: *Mt*, *Medicago truncatula* [G7KRM5], *Mt_2* indicates the second isoform of *Mt*P5CR [A2Q2Y7]; *At*, *Arabidopsis thaliana* [P54904]; *Os*, *Oryza sativa* [Q8GT01]; *Ps*, *Pisum sativum* [Q04708]; *Gm*, *Glycine max* [K7KEQ2]; *So*, *Spinacia oleracea*, only partial sequence is available (Murahama et al., 2001); *Hs*, *Homo sapiens* [P32322]; *Sp*, *Streptococcus pyogenes* [Q9A1S9]; *Nm*, *Neisseria meningitidis* [Q9K1N1]. Amino acid residues are colored according to the type of residue. Numbering on the top reflects the *Mt*P5CR sequence, while that on the right of each row is protein-specific. Residues interacting with NAD(P)⁺ and L-proline in *Mt*P5CR structure and conserved among other species are highlighted in gray and light blue, respectively. α -Helices, 3_{10} helices and β -strands corresponding to *Mt*P5CR structure are depicted on top as red, blue and yellow bars, respectively. L1, L3, and L19 indicate the location of loops 1, 3, and 19, which were discussed in the paper. Seven C-terminal residues from the human P5CR sequence were omitted. The human and the two bacterial sequences were chosen for alignment as their crystal structures had already been determined.

are organized in such way that the N-terminal domains point outwards of the hollow core of the decamer. As a result, a large groove around the decamer is formed in a plane perpendicular to the five-fold NCS axis. Each N-terminal domain is an $\alpha/\beta/\alpha$ sandwich of a nucleotide-binding Rossmann fold composed of

eight helices wrapped around an eight-stranded β -sheet. The organization of strands within the β sheet is as follows: β 3- β 2- β 1- β 4- β 5- β 6- β 7*- β 8* (where an asterisk indicates the opposite direction of the strand). Between the strands β 6 and β 7*, a β -hairpin is formed that contains a 3_{10} helix (η 7). There are four

TABLE 2 | Kinetic features of *Medicago truncatula* P5CR.

| | |
|-----------------------------------|--------------------------------------------------|
| $K_{M(\text{app})}$ L-P5C (NADH) | $240 \pm 24 \mu\text{M}$ |
| $K_{M(\text{app})}$ L-P5C (NADPH) | $20 \pm 2 \mu\text{M}$ |
| $K_{M(\text{app})}$ NADH | $468 \pm 22 \mu\text{M}$ |
| $K_{M(\text{app})}$ NADPH | $39 \pm 3 \mu\text{M}$ |
| V_{max} L-P5C (NADH) | $97.8 \pm 4.7 \mu\text{kat (mg protein)}^{-1}$ |
| V_{max} L-P5C (NADPH) | $35.1 \pm 0.8 \mu\text{kat (mg protein)}^{-1}$ |
| V_{max} NADH | $92.4 \pm 2.1 \mu\text{kat (mg protein)}^{-1}$ |
| V_{max} NADPH | $36.1 \pm 0.7 \mu\text{kat (mg protein)}^{-1}$ |
| k_{cat} (NADH) | 2972 s^{-1} |
| k_{cat} (NADPH) | 1113 s^{-1} |
| k_{cat}/K_M (NADH) | $6.35 \times 10^6 \text{ M}^{-1} \text{ s}^{-1}$ |
| k_{cat}/K_M (NADPH) | $2.85 \times 10^7 \text{ M}^{-1} \text{ s}^{-1}$ |



fragments within the N-terminal domain that have a 3_{10} helix twist (η_2 , η_3 , η_5 , η_7 ; numbering of the helices is consecutive, regardless of their type).

The C-terminal domain of *MtP5CR* consists of six helices and includes a hinge that probably allows for independent movement of the N-terminal domains in solution. This hinge results in a triple deformation of the ninth helix: (i) a tight 3_{10} helix (η_9), (ii) backbone torsion angles of Leu178 outside the expected range, and (iii) a break between the α_9 and α_{10} helices at Gly180. The C-terminal domains are responsible for incorporating two monomers into a dimer. More precisely, five C-terminal helices (α_{10} – α_{14}) are swapped between the monomers within the dyad and form a multi-helix bundle. The surface areas of isolated monomers and dimers equal $12,380$ and $19,560 \text{ \AA}^2$, respectively. Hence, the calculated buried surface area upon dimer formation is extensive, equaling 5200 \AA^2 . Each C-terminal domain also contains the P5C binding site that is the reduction reaction venue.

MtP5CR, like other plant P5CRs, shares a higher sequence identity with the human ortholog than with the bacterial ones (Forlani et al., 2015b). Interestingly, from the structural alignment (Figure 6) it appears that *MtP5CR* is actually more similar to *SpP5CR* [PDB ID: 2ahr, (Nocek et al., 2005); root-mean-square deviation (RMSD) 1.6 \AA] and *NmP5CR* (2ag8, (Nocek et al., 2005); RMSD 1.5 \AA) than to human P5CR (2izz, Pike et al., unpublished, RMSD 1.9 \AA).

Most of the differences are noticeable within the N-terminal domain and apply to the helices. More precisely, the η_3 and the α_6 helices that in *MtP5CR* are similar to bacterial orthologs have different inclinations in the human protein. On the other hand, the 5th helix of the *MtP5CR* enzyme is longer (by the η_5 fragment) than the corresponding helices in the two prokaryotic P5CRs, and resembles the corresponding helix of the human ortholog. The NAD(P)⁺ is bound in each of the four compared structures in a similar way (Figure 6) and, when the protein chains are superposed, the corresponding atoms of the coenzymes deviate by less than 3.5 \AA . The major difference concerning the C-terminal domain is the break between helices α_9 and α_{10} , which is observed in the *Mt*, *Hs* and *Nm* enzymes, but is absent in the *Sp* ortholog. *NmP5CR* is a dimer in solution (Nocek et al., 2005), while *Sp*, *Hs*, and *Mt* enzymes are decamers. Therefore, the break between helices α_9 and α_{10} is unrelated to oligomerization.

Pyridine Dinucleotide Binding is Consistent with the Preference for NADPH over NADH as the Electron Donor

The catalytic centers of P5CRs are located between the dinucleotide-binding domain (N-terminal) and the dimerization domain (C-terminal) (Nocek et al., 2005). However, the substrates and the coenzymes are delivered to the catalytic centers by different protein subunits that form the dimer. In other words, P5C bound by the C-terminal domain of protein subunit A is reduced by NAD(P)H brought by the N-terminal domain of its dimer mate, subunit B. The reaction can occur in the second active site within the dimer simultaneously, namely the hydride provided by NAD(P)H bound by subunit A can reduce P5C to L-proline in the active center of subunit B.

Close examination revealed an electron density matching of L-proline surrounded by the L19 loop, between Ser238 and Thr242 in each of the 10 chains of the *MtP5CR*/L-proline complex (Figure 7). The reaction product interacts with the protein chain through both carboxyl O atoms. The O1 atom, at an *anti* position with respect to N of L-proline, forms hydrogen bonds with the backbone N of Thr242 and O γ of the same residue. The O2 atom (*syn* to N of L-Pro) interacts with O γ of Ser238, O γ of Thr243 and a well-ordered water molecule at the bottom of the cavity. This water molecule is hydrogen-bonded to the carbonyl O of Ser238 and the backbone N of Ile244. The N atom of proline participates in product binding through formation of a weak hydrogen bond with O γ of Thr243.

Concerning hydride donors, the complexes with NAD⁺ and NADP⁺ showed that both coenzymes are bound by the N-terminal domain of *MtP5CR* via multiple hydrogen bonds

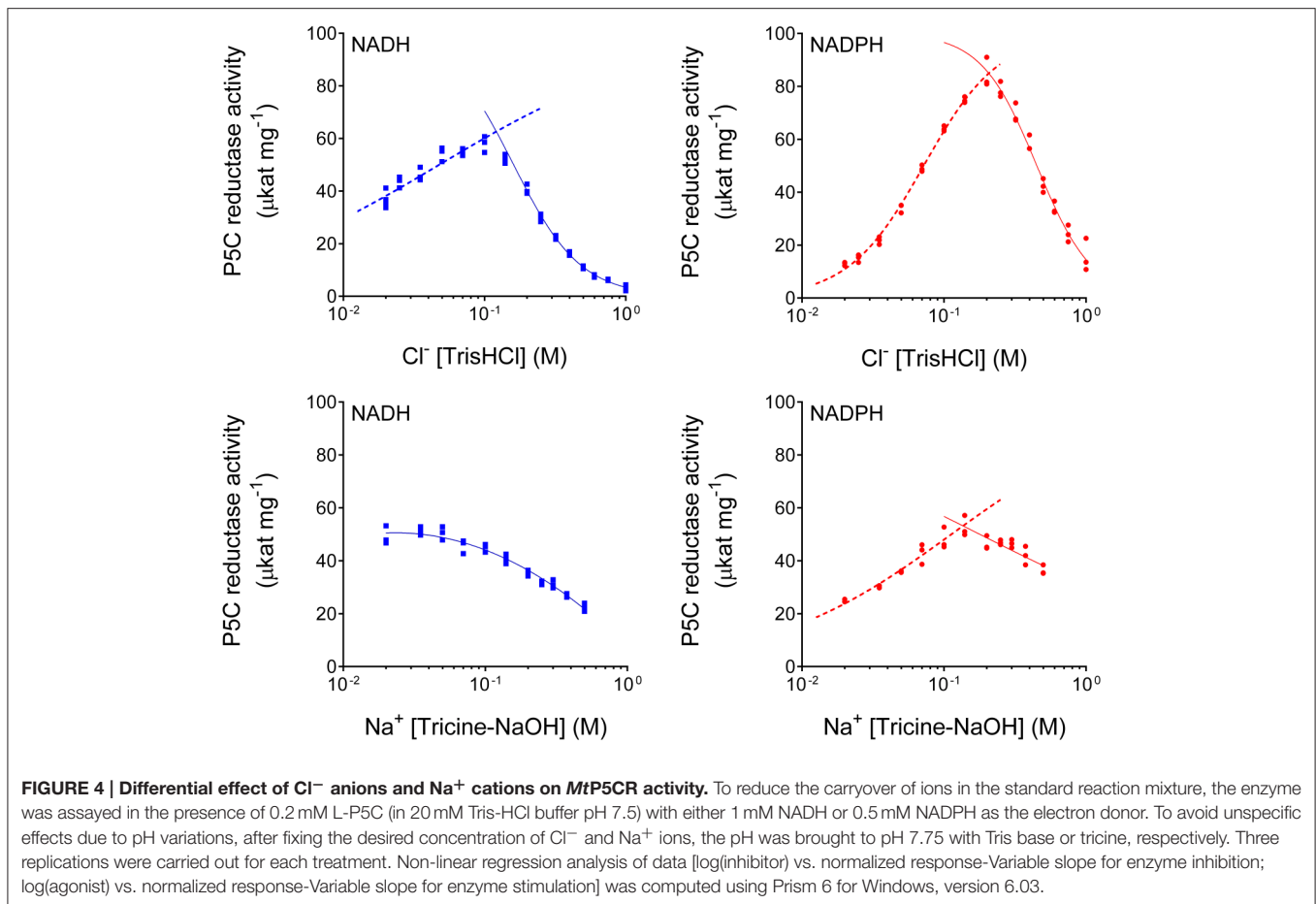
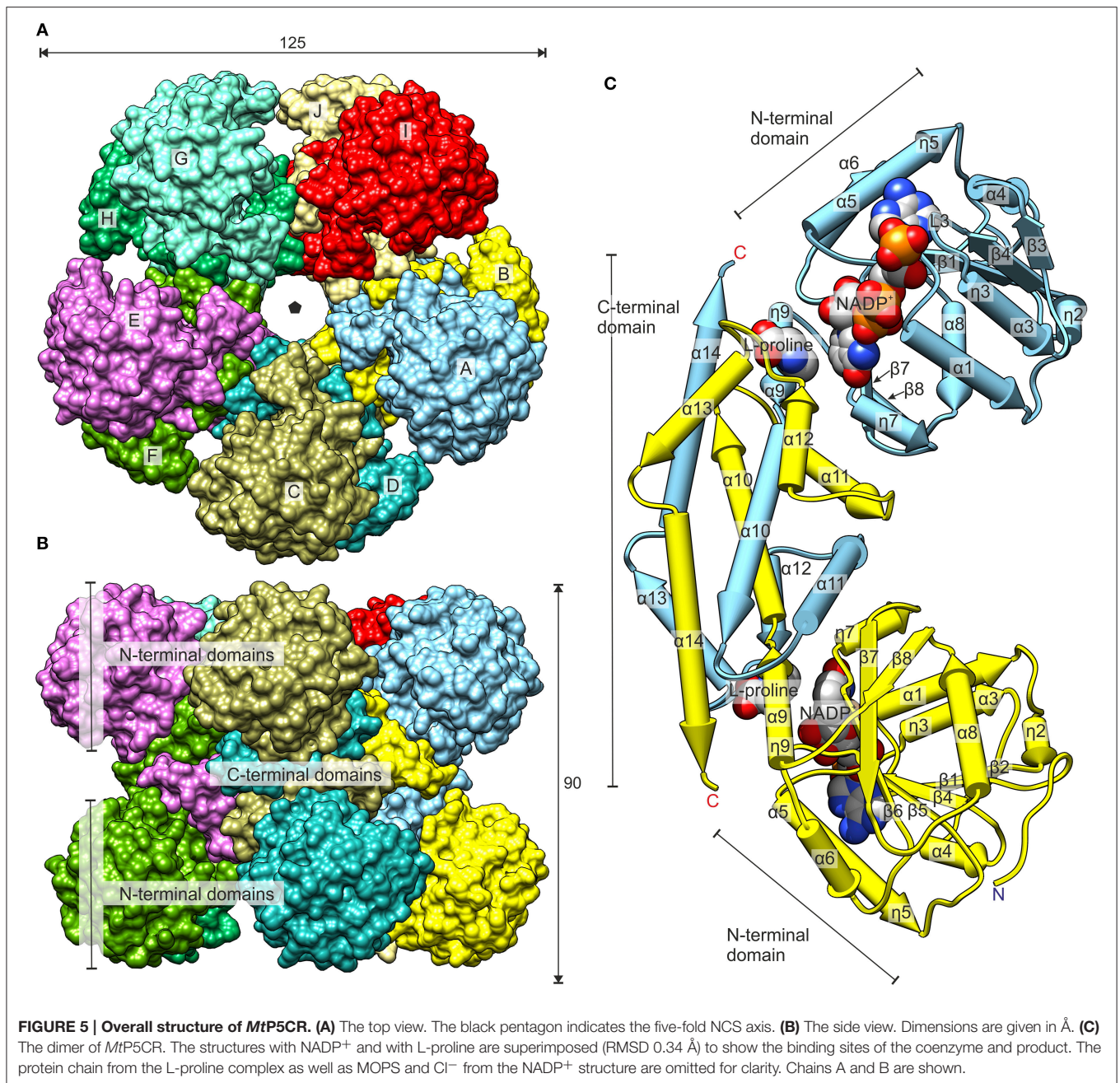


(Figure 8) created mostly by the backbone N and O atoms of the protein. The coenzyme-binding groove contains the dinucleotide-binding motif of the Rossmann fold, which, in the case of *Mt*P5CR, encompasses residues ₁₇GAGKMA₂₂, which correspond to the L1 loop and the N-terminal part of α 1 helix.

In the case of NAD⁺ (Figure 8A), the adenine N1 atom interacts with N δ of Asn65. The N3 atom of adenine forms water-mediated hydrogen bonds with the backbone N and O of Ala18 and Ala43, respectively. The binding of the N6 atom by the backbone O atoms of Leu83 and Val87 occurs *via* two solvent molecules in both cases. Additionally, adenine interacts by π -stacking to His45 with an interplanar distance of about 3.6 Å and an inclination below 6°. The adenine-adjacent ribose interacts *via* a single water-mediated hydrogen bond between the O atom of the monosaccharide and the backbone N atom of Lys80. The O atoms of the pyrophosphate group form strong ionic hydrogen bonds to the peptide amides of Lys20, Met21 and, *via* H₂O, to Gly19 and Ala22. The overall dipole moment of helix α 1, of which Lys20, Met21, and Ala22 are the N-terminal residues, also contributes to the increased electrostatic attraction. Additionally, the pyrophosphate interacts with the N ζ atoms of Lys20 and Lys80. These N ζ atoms are not well-defined in the electron density maps; they may, perhaps, bind

with similar energies to various O atoms of pyrophosphate. These fully exposed Lys20 and Lys80 residues may act like claws that capture the coenzyme by its pyrophosphate moiety and seize the coenzyme from the solvent/cytoplasm at the initial stage of binding. These two residues are highly conserved in different species (Figure 2). The nicotinamide-adjacent ribose forms two direct hydrogen bonds between O2' and the backbone NH of Ala106, as well as between O3' and the carbonyl of Val79. The nicotinamide interacts *via* a water molecule with O γ of Thr129. In addition, an intramolecular hydrogen bond between the amide N atom of nicotinamide and one of the pyrophosphate oxygens allows for determination of the correct orientation of the amide group. The *si*-side of the C4 carbon atom of the nicotinamide faces toward the catalytic center. This means that during the reduction reaction, the hydride would be transferred from the *pro*-S position of NAD(P)H (Figure 7).

NADP⁺ is bound in a very similar manner to NAD⁺ (Figure 8B), though differences arise from the presence of the additional phosphate group bound to O2' of the adenine-adjacent ribose. This phosphate group causes rearrangement of the L3 loop (₄₄IHSNP₄₈) and contributes to a higher number of binding interactions. The three oxygen atoms of the phosphate group create ionic hydrogen bonds with: (i) the backbone N atoms of Ser46 and Asn47 and O γ of Ser46 (O1 of phosphate), (ii) the N δ

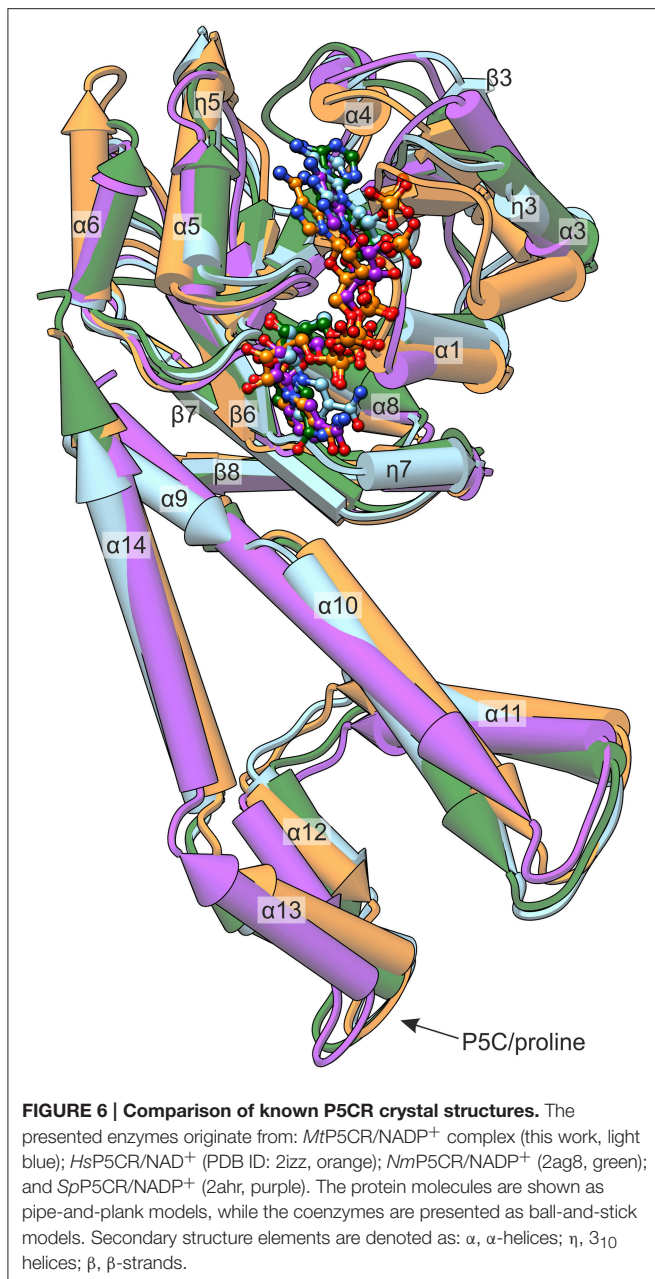


atom of His45 (O2), and (iii) the N8 atom of Asn47 (O3). One additional interaction occurs between the N7 atom of the adenine moiety and the water molecule that ultimately (by another water molecule) binds to carbonyl O of Leu83.

Anions but not Cations are Present in the Active Site of *MtP5CR*

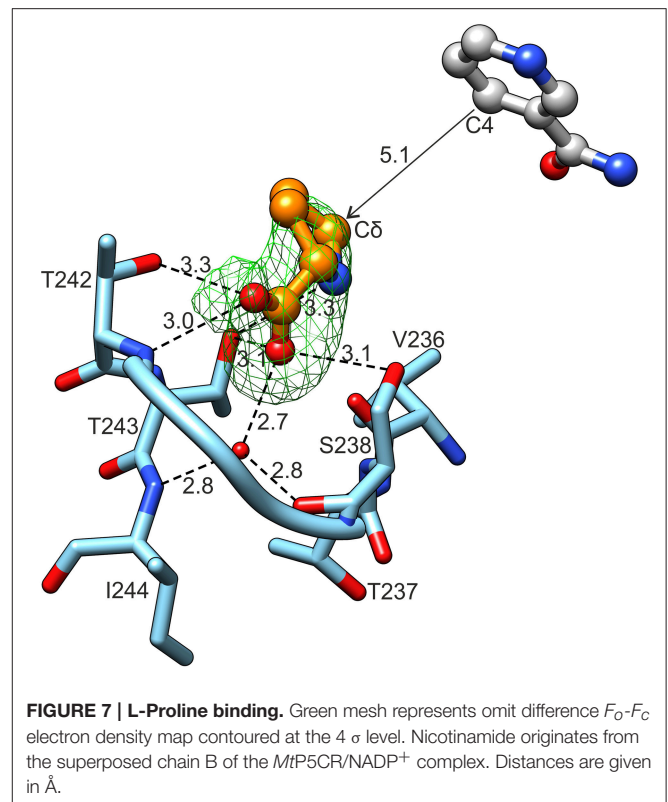
MtP5CR crystallized in the presence of Mg²⁺ and Ca²⁺, but neither cation was found in the electron density maps of *MtP5CR* structures. On the contrary, in the crystal structures of unliganded *MtP5CR* and both holo complexes, chloride anions

are present in the catalytic center (**Figure 9A**). Examination of the vicinity of the chlorides revealed up to seven (chain- and structure-dependent) H-bonding interactions that, in the complex with L-proline, are distributed between its two carboxyl O atoms. Up to four of these bonds are formed with N atoms. Also, highly positive peaks in $F_o - F_c$ electron density maps appear if a water molecule is placed instead of the chloride, suggesting a larger atom. The presence of chlorides was verified with the use of anomalous difference electron density map, resulting from diffraction data collected at 1.7196 Å wavelength (**Figure 9A**).



Binding of Anions that Partially Overlap with the Proline Binding Site can Result in Inhibition of *MtP5CR* Activity

In the catalytic center of the enzyme, a MOPS molecule was also found in the structures with either coenzyme. Superposition of *MtP5CR* structures complexed with L-proline and NAD(P)⁺ revealed that such a molecule is located between the product and the coenzyme (Figure 9B). In each case it is stabilized by a single hydrogen bond between the O atom from a MOPS sulfate group and O2' of the nicotinamide-adjacent ribose. Upon superimposition with the *MtP5CR*/L-proline complex, the morpholine ring of MOPS partially overlaps with proline,



although not interacting with the protein residues that establish contacts with the amino acid. As a result, the distance between the nicotinamide C4 atom of NAD(P)⁺ and C δ of proline in the superposed structures is about 5.1 Å, whereas in the structure from *S. pyogenes* this distance is about 3.3 Å (Nocek et al., 2005).

Because of its positioning inside the catalytic center of *MtP5CR*, the effect of increasing concentrations of MOPS on enzyme activity was evaluated. Quite surprisingly, in the 1–100 mM range MOPS did not cause any significant inhibition. However, another commonly used sulfonic buffering agent, HEPES, progressively inhibited both the NADH- and the NADPH-dependent activity of the enzyme, with an IC₅₀ value of 3.0 ± 0.2 mM. Kinetic analyses (Figure 10) were consistent with inhibition by a non-competitive mechanism with respect to all substrates, with K_I values of 1.83 ± 0.08 , 1.91 ± 0.06 , 2.84 ± 0.17 , and 3.10 ± 0.36 mM for NADH, NADPH, P5C_(NADH), and P5C_(NADPH), respectively.

DISCUSSION

The Availability of the Three-dimensional Structure of Plant P5CR Allows a Better Comprehension of the Catalytic Mechanism and the Regulatory Interactions that Modulate its Activity

This is the first paper to describe the structural characterization of P5CR from a plant. Four crystal structures -unliganded

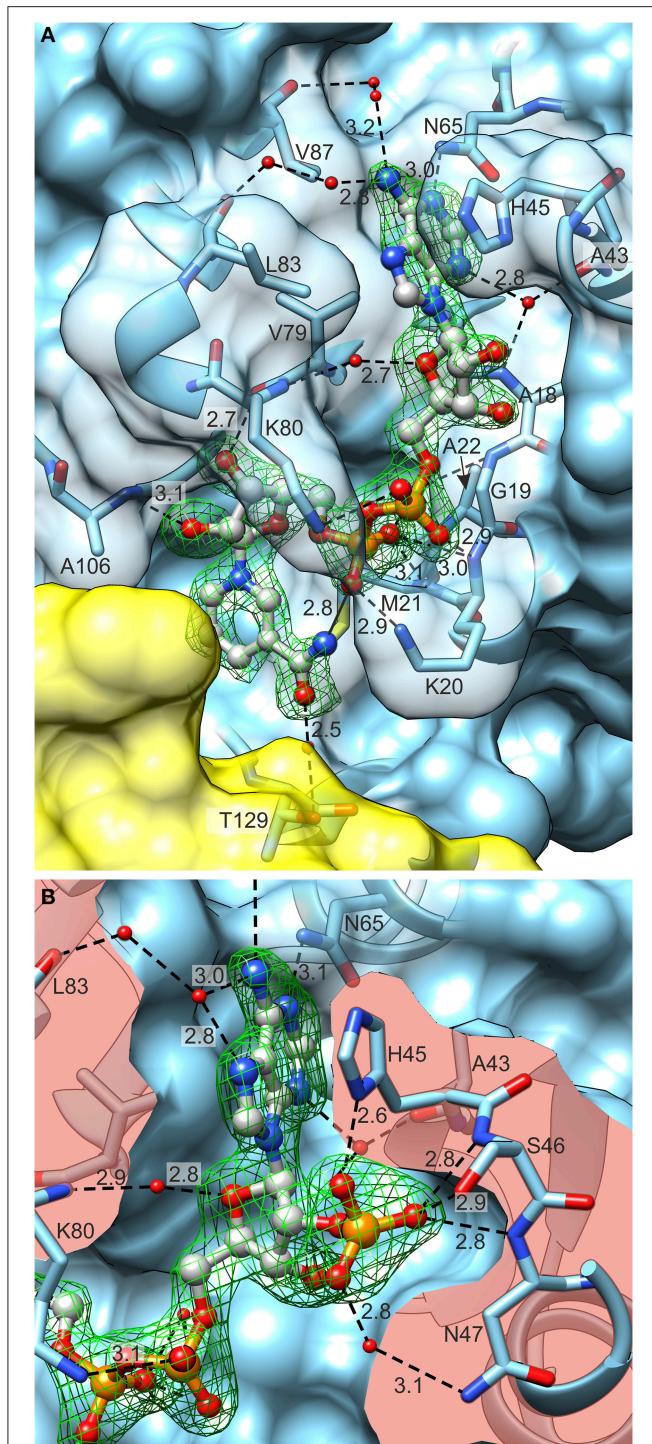


FIGURE 8 | Coenzyme (ball-and-stick model) binding by *MtP5CR*.

(A) The *MtP5CR*/NAD⁺ complex. **(B)** The close-up view of the ribose 2'-O-bound phosphate in NADP⁺. Both figures are oriented as in **Figure 1C**. Green mesh areas represent omit difference $F_o - F_c$ electron density maps contoured at the 4 σ level. Water molecules that take part in binding interactions are depicted as small red balls. Chain B is represented as a yellow semitransparent surface. Note that Thr129 belongs to chain A and is only covered by a part of the C-terminal domain of chain B. The surface of interacting amino acids is semitransparent in **(A)** and clipped in **(B)** so it does

FIGURE 8 | Continued

not obscure the coenzymes. Black dashed lines represent bonding protein-coenzyme interactions. Intramolecular interaction between the N atom of nicotinamide and O from pyrophosphate group of NAD⁺ is depicted as a black solid line at the bottom of **(A)**. Distances are given in Å.

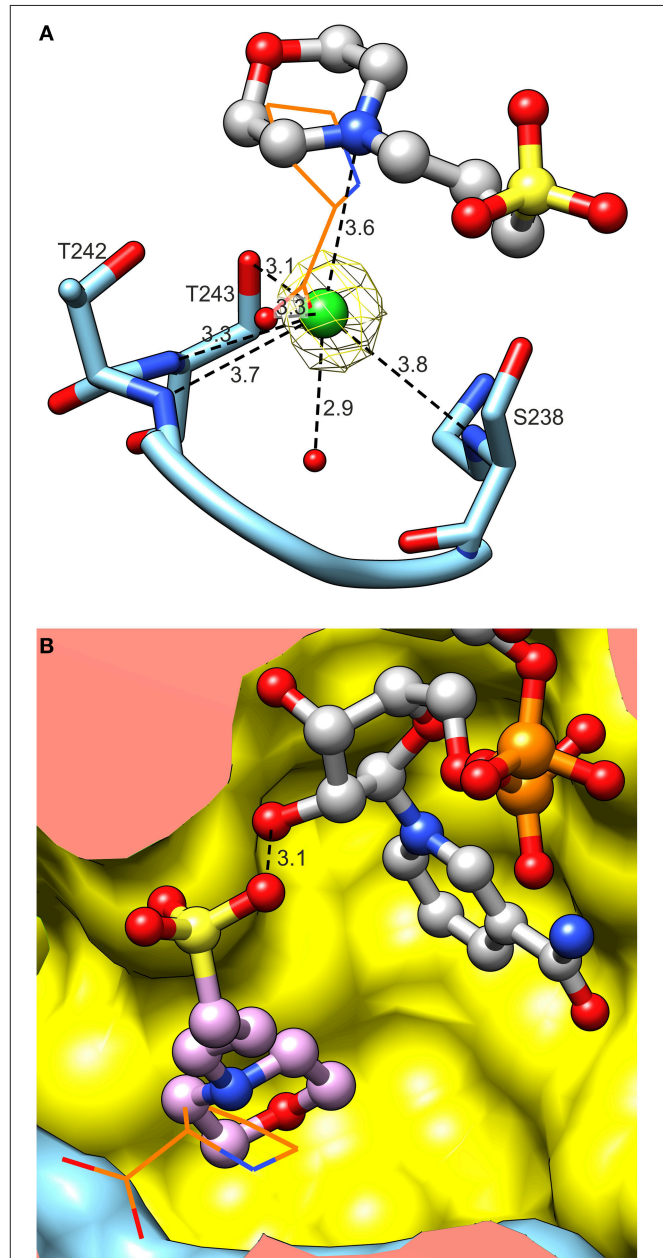


FIGURE 9 | Binding of activity modulators. (A) Binding of chloride in the active site. Note multiple hydrogen bonds between Cl⁻ and peptide amides. Yellow mesh represents anomalous difference electron density map contoured at 4 σ . Superposed L-proline (from the *MtP5CR*/L-proline complex, wires) is shown to visualize the Cl⁻ overlapping the carboxyl O. **(B)** Superposition of *MtP5CR*/L-proline and *MtP5CR*/NAD(P)⁺ complexes reveals that the MOPS molecule (originating from NAD(P)⁺ complexes) partially overlaps with L-proline (wires).

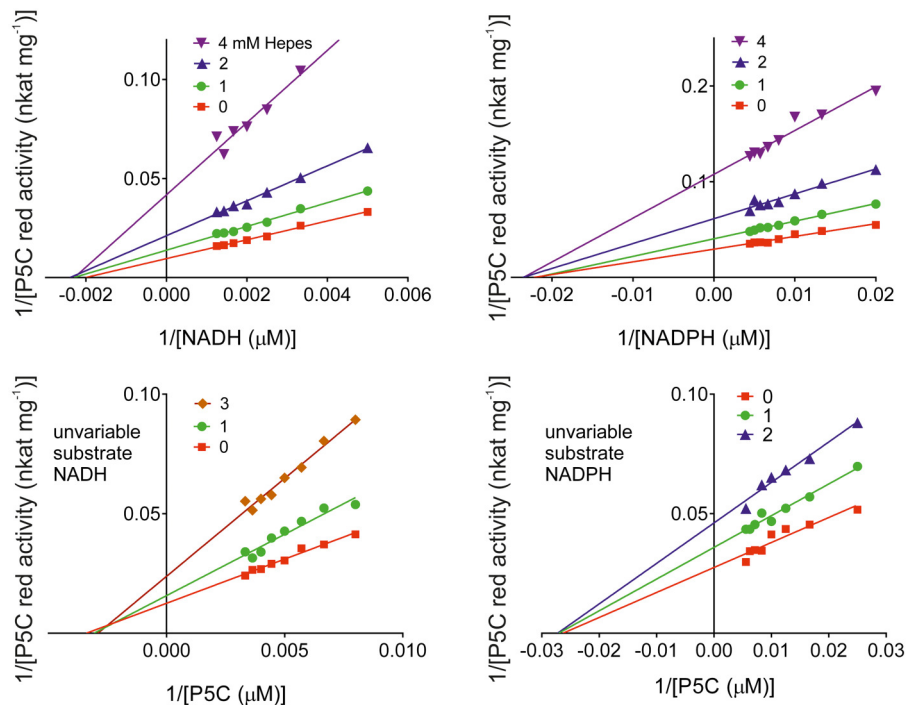


FIGURE 10 | Kinetic analysis of the inhibition of *MtP5CR* by HEPES. Enzyme activity was measured at varying substrate concentrations in the presence of various inhibitor levels. Invariable substrates were fixed as in the standard mixture. Three replications were carried out for each treatment. Lines intersecting at the x-axis in the Lineweaver-Burk plots accounted for non-competitive inhibition types in all cases. Non-linear regression analysis of data [Michaelis-Menten fit, Lineweaver-Burk (double-reciprocal) transform, linear regression over Michaelis-Menten data, and non-competitive inhibition] was computed using Prism 6 for Windows, version 6.03.

MtP5CR, its complexes with NAD^+ and NADP^+ and its complex with L-proline revealed a structural model for the *M. truncatula* enzyme. Given that the plant proteins share a high level of sequence similarity (Forlani et al., 2015b; this work, **Figure 2**), at least part of these results can be extrapolated to other plant species. Indeed, with the only exception of the sensitivity to product inhibition by proline, also the biochemical and kinetic properties of *MtP5CR* were found similar to those recently pointed out for the enzyme from *A. thaliana* (Giberti et al., 2014) and *O. sativa* (Forlani et al., 2015a).

For this study, the reaction product (L-proline) was used instead of the substrate (L-P5C) to determine the active site of *MtP5CR*, due to the high lability of P5C at neutral pH values (Williams and Frank, 1975). Upon binding, the N atom of proline forms a weak hydrogen bond with O_γ of Thr243. It is, however, possible that P5C can create a different interaction involving its N atom. This is because the imine N atom in P5C has sp^2 hybridization, which means that the N-bound hydrogen would point toward the carbonyl of Val236 and contribute to increased affinity for P5C vs. L-proline. This interaction could explain why *MtP5CR* and some other P5CRs are not subjected to product inhibition by L-proline (Merrill et al., 1989; Petrollino and Forlani, 2012). Higher affinity for the substrate than for the product would be very beneficial, as proline may be very abundant in the cell, mainly under stress conditions. The crystal structure of the

only other P5CR/L-proline complex available to date, that of *SpP5CR* (Nocek et al., 2005), strengthens the hypothesis that in the active site of *MtP5CR* P5C can interact with the carbonyl of Val236 (Ile219 in *SpP5CR*). It would be of great interest to verify whether structural differences favoring or disfavoring this interaction may discriminate proline-insensitive P5CRs [the human PYCR1 (Meng et al., 2006), *SpP5CR* (Nocek et al., 2005), *MtP5CR* (this work)] from those that are susceptible to proline inhibition, at least when NADH is the electron donor [the human PYCR2 (Merrill et al., 1989; Meng et al., 2006), *AtP5CR* (Giberti et al., 2014), *OsP5CR* (Forlani et al., 2015a)]. Unfortunately, however, a three-dimensional structure showing a detailed proline binding mode by a proline-sensitive P5CR is still unavailable.

Because of the presence of a MOPS molecule in both complexes with coenzymes, interpretation of the reaction mechanism based on the presented structures is not straightforward. It is, however, possible to analyze the substrate and coenzyme binding order. According to Nocek et al. (2005), in the *SpP5CR*/L-proline complex the entrance to the catalytic center is blocked when a coenzyme is bound by the N-terminal domain. Therefore, P5C would be required to be bound prior to NAD(P)H . However, from crystal structures of *MtP5CR*/ NAD(P)^+ complexes we learn that the channel leading to the P5C-binding cavity is relatively wide (about 10 Å). This means that, at least in *MtP5CR*, the substrate can easily penetrate

its way to the catalytic center of a protein molecule whose dimer mate has already bound the coenzyme.

Consistent Kinetic and Structural Data Suggest That NADPH May Be the Only Electron Donor *in Vivo*

P5CRs from most sources were reported to be able to use *in vitro* either NADH or NADPH as the coenzyme, with contrasting affinity and maximal activity. However, recent biochemical data questioned the possibility that NADH can be used *in vivo* (Giberti et al., 2014; Forlani et al., 2015a). The present results strengthen this conclusion, as the highly conserved L3 loop was found to strongly interact with the O2'-ribose phosphate group of NADP⁺, implying a higher affinity for NADPH. Since the crystallization is a long-term experiment, the oxidized, more stable forms of the dinucleotides were used instead of the hydride donors. Both NAD⁺ and NADP⁺ coenzymes are bound by the N-terminal domain of *MtP5CR*. The description of binding modes is based on chains A, as they have the best-quality electron density maps for the L3 loops. Nevertheless, a majority of the binding contacts are preserved in other subunits and the small discrepancies can be attributed to different solvent exposures within the crystal lattice. The L3 loop is the most flexible structural element of *MtP5CR*. In apo structures (unliganded and complexed with L-proline) loop L3 occupies a part of the coenzyme-binding site. Moreover, in these two complexes the imidazole ring of His45 lies in a structural position similar to that of adenine from NAD(P)⁺. Binding of a coenzyme undoubtedly stabilizes the L3 loop, and this effect is most evident when NADP⁺ is bound.

Interestingly, the sequence of the L3 loop is highly conserved among plant P5CRs (Figure 2), especially a histidine residue at position 45 (in *MtP5CR*), which is present in all compared plant orthologs. It is worthy to note that the corresponding sequence motif in rice has even more positively charged residues that could interact with the phosphate of NADPH. Consistently, the difference between the sensitivity to NADP⁺ of the NADH-dependent and the NADPH-dependent activity is higher for the rice enzyme (103-fold; Forlani et al., 2015a) than for *MtP5CR* (26-fold; Figure 3). Even though in the spinach P5CR the histidine is the only amino acid able to carry positive charge and serve as H-bond donor within the L3 loop, the enzyme showed a 10-fold lower K_M for NADPH than for NADH (Murahama et al., 2001). As a consequence, NADP⁺ strongly inhibits the P5C-to-proline conversion if NADH was used as the coenzyme, whereas it is almost ineffective at physiological concentrations when NADPH is the electron donor. In alfalfa (*Medicago sativa*), NADH and NADP⁺ concentrations of 9 and 37 nmol g⁻¹ (fresh weight), respectively, have been found, whereas the NADPH/NADP⁺ ratio was approximately equal to unity (Igamberdiev et al., 2004). Similar ratios have been reported in other plant species (Hayashi et al., 2005; Takahashi et al., 2009). Under these conditions, and also taking into account the high K_M values for NADH and P5C_(NADH) (Table 2), the NADH-dependent activity would therefore be negligible. This may solve substrate ambiguity, as it suggests that *in vivo*

MtP5CR most likely relies entirely on NADPH as the reducing agent.

A preferential use of NADPH over NADH may have some important implications *in planta*, assuming P5CRs are also present in chloroplasts (Rayapati et al., 1989; Murahama et al., 2001). As a result of P5C-to-proline conversion, NADP⁺ is produced. In chloroplasts, NADP⁺ can enter the OPPP, which not only regenerates ribulose-5-phosphate, but also provides fresh NADPH and CO₂ (Kohl et al., 1988). Production of carbon dioxide is particularly beneficial during water stress conditions, when the stomata are closed, which adversely impacts CO₂ assimilation. Therefore, owing to P5CR activity, photosynthesis can proceed and the plant does not suffer from either photoinhibition (Hideg et al., 1998) or excess reactive oxygen species in the chloroplast. However, the subcellular location of P5CRs *in planta* is still under debate, as no universal pattern has been determined. Studies on soybean (*Glycine max*) revealed P5CR activities in both cytosol and plastid fractions (Kohl et al., 1988; Szoke et al., 1992), while the enzyme from pea (*Pisum sativum*) (Rayapati et al., 1989) and the spinach P5CR isozyme 2 (Murahama et al., 2001) were located in chloroplasts.

Anions but not Cations Seem Likely to Modulate *MtP5CR* Activity

The effects of Cl⁻ ions on *MtP5CR* activity were evaluated by *in vitro* tests, which showed that high concentrations of chlorides are inhibitory. Conversely, low chloride concentrations had a stimulatory effect on the NADPH-dependent activity. These results are consistent with those recently obtained using P5CRs from *A. thaliana* (Giberti et al., 2014) and rice (Forlani et al., 2015a), although in those cases enzyme stimulation by chlorides was found only with NADPH as the electron donor. Such a feature is extremely interesting from a physiological point of view, since it provides a rapid way to increase hyperosmotic stress-induced proline synthesis in the presence of excess chlorides in the cytosol, without the need for transcriptional control of P5CR expression. However, the mechanism by which Cl⁻ exerts its action has never been explained before. In the crystal structures of unliganded *MtP5CR* and both holo-complexes, chloride anions were found in the catalytic centers at the same structural positions as the carboxyl groups of L-prolines in the *MtP5CR*/L-proline complex (Figure 9A). Therefore, as inferred from the crystal structures, chloride ions should be rather inhibitory as they compete for the same site with the carboxylic group of L-proline and, most probably, P5C. Indeed, the concentration of Cl⁻ ions in the crystallization drop when the crystals were harvested should have exceeded 340 mM. As a consequence, we propose that the Cl⁻ found in the crystal structure reflects the inhibitory role of Cl⁻.

It is, on the contrary, difficult to determine the mechanism of stimulation of enzyme activity by a low concentration of chloride ions because there are no more Cl⁻ binding sites found in the crystal structures of *MtP5CR*. The stimulatory Cl⁻ could bind to the same site and, in that way, keep the L-proline (and P5C) binding site, the L19 loop, properly arranged (Figure 9A). Perhaps, in the absence of Cl⁻, the loop incorporates a water

molecule, changes conformation and becomes unable to bind P5C. In that scenario, it would be only a matter of shifting equilibrium, where at low (stimulatory) concentrations of Cl^- the P5C can enter the reaction venue, whereas at high (inhibitory) concentrations the halogen prevents P5C from entering. This is, however, merely speculation, and additional tests, e.g., with other Na-halogen salts that would differently modify the L19 loop, will be required to shed further light on the mechanism. *In planta*, where local chloride concentrations in the range of 25–100 mM can be considered physiological in salt-stressed plants (Britto et al., 2004), only the *stimulatory* role of chloride ions seems relevant. On the contrary, chloride concentrations at which *MtP5CR* activity is inhibited are far from occurring even in plants exposed to extreme salinity.

On the other hand, and despite their presence in the crystallization medium, neither Mg^{2+} nor Ca^{2+} ions were found in the electron density maps of *MtP5CR* structures. Interestingly, both cations were reported as inhibitors of P5CR from spinach, against which divalent cations were found stronger inhibitors than monovalent cations (Murahama et al., 2001). However, in that study all cations were added as chloride salts. It is, therefore, impossible to distinguish between what actually worked as an inhibitor, the divalent cations or the chloride anions, especially when divalent salts dissociate to double the Cl^- concentration. Additionally, the divalent cations are intrinsically prone to complexing with the pyrophosphate group of NAD(P)H, and metal-complexed NAD(P)H cannot enter the binding site. Consistently, in the case of spinach P5CR, ATP was found inhibitory by competing with NAD(P)H, and the inhibition was partially mitigated when MgCl_2 was also added (Murahama et al., 2001). Most likely, in that case some ATP complexes with Mg^{2+} cations and, therefore, ATP cannot bind to the NAD(P)H binding site and cannot inhibit P5CR.

The Presence of Anions in the Catalytic Center and their Effects on Enzyme Activity Provide a New Lead for the Development of Effective Inhibitors of P5CR Activity

In the complexes with either coenzyme, a MOPS molecule was found in the catalytic center of the enzyme. As a result, the distance between the nicotinamide C4 atom of NAD(P)⁺ and C δ of proline in the superposed structures increases from 3.3 Å in *SpP5CR* (Nocek et al., 2005) to about 5.1 Å. A short distance should allow *in vivo* a direct transfer of the hydride from the *pro-S* face of C4 of NAD(P)H to C5 of P5C. To verify this hypothesis for *MtP5CR*, a different crystallization condition, without MOPS buffer, needs to be developed. It is possible, however, that binding of MOPS actually enables the crystal formation, as it forces the protein molecules to adopt the same conformation. Only in the structure with L-proline, which was obtained *via* soaking, MOPS is not present, but its coenzyme-binding domain is shifted by less than 0.4 Å when compared to the NAD(P)⁺-bound complexes. Apparently, prior to soaking the protein molecules had adopted the crystallization-promoting conformations, which were maintained by inter-decamer contacts in the crystal lattice and were not changed by subsequent product binding.

Whatever the mechanism, the binding of anions near the L-proline binding site may have interesting practical applications. The addition to the assay mixture of MOPS concentrations up to 100 mM was found ineffective. However, when HEPES was used instead, which bears a larger 2-[4-(2-hydroxyethyl)piperazin-1-yl]ethane moiety than the 3-morpholinopropane moiety of MOPS, a significant inhibition of enzyme activity was found. On the whole, the inhibitory effect is mild, and evident only at relatively high concentrations. However, the mechanism of the inhibition by HEPES is very interesting because, as a non-competitive inhibitor, it does not depend on the concentration of enzyme substrates.

Being placed at the converging point of the two pathways leading to proline synthesis in plants and most microorganisms, P5CRs are attractive targets for the development of either new therapeutics (Forlani et al., 2012) or new active ingredients for weed control (Forlani et al., 2007, 2008). Several recently identified aminomethylene-bisphosphonic acids are able to inhibit plant P5CRs at micromolar concentrations. However, the most active compounds showed an uncompetitive type of mechanism with respect to P5C (Forlani et al., 2007). As a consequence, they would be most effective in the presence of saturating levels of P5C, which is, on the contrary, maintained at very low concentrations inside the cell (Forlani et al., 2013) to avoid cytotoxic effects (Deuschle et al., 2004). In the presence of limiting P5C concentrations, interaction with such inhibitors results in a higher affinity for the substrate. This would cause a lower effectiveness *in vivo* than *in vitro*. Moreover, because the crystal structure of the plant enzyme was unavailable at the time, aminophosphonate inhibitors were designed using a computer-aided docking procedure performed on the basis of the crystal structure of the enzyme from *S. pyogenes* (Nocek et al., 2005). Consistently, the susceptibility of the bacterial enzyme has been found to be strikingly higher than that of the plant P5CR, with IC₅₀ values differing by 2–3 orders of magnitude (Forlani et al., 2012, 2013). The present results, therefore, provide new information on these aspects, and point at the alkylsulfonic acid moiety as a new lead for the development of specific inhibitors targeting plant P5CR.

CONCLUSIONS

This work was focused on description of the main features of a plant P5CR from a functional and structural perspective. The enzyme from the model legume, *Medicago truncatula*, was chosen for the study. Four crystal structures (unliganded *MtP5CR*, its complexes with NAD⁺, NADP⁺, and L-proline) were solved and provided a structural model for the protein. Even though P5CR sequences differ between species from different domains of life, we showed that the overall fold of *MtP5CR* is similar to those of the bacterial and human orthologs, which have had their three-dimensional structures determined (Nocek et al., 2005; Pike et al., unpublished).

The coenzyme preference for NADPH over NADH, reported previously for other plant species (Szoke et al., 1992; Murahama et al., 2001; Giberti et al., 2014) based on enzymatic assays, was confirmed and interpreted for the first time from the

structural point of view. The highly conserved L3 loop was found to strongly interact with the phosphate group connected to O2'-ribose of NADP⁺, implying a higher affinity for NADPH. This observation was also supported by enzymatic assays, which showed a 12-fold lower $K_{M(\text{app})}$ value for NADPH than for NADH. Moreover, NADP⁺ was found to strongly inhibit the P5C-to-proline conversion if NADH was used as the coenzyme, whereas NADP⁺ was almost ineffective at physiological concentrations when NADPH was the hydride donor. NAD⁺ did not exert any inhibitory effect regardless of the coenzyme used. Therefore, considering the physiological concentrations of reduced and oxidized forms of both coenzymes, it is highly unlikely that NADH could serve as the reductant *in vivo*.

Last, but not least, the effects of chloride ions, MOPS, and HEPES molecules on the enzyme activity were tested. Chloride ion was found to occupy the same position as the carboxyl group of L-proline. In *in vitro* tests low concentrations of chloride ions had a remarkable stimulatory effect on the NADPH-dependent activity, whereas high Cl⁻ concentrations inhibited *MtP5CR*. Interestingly, HEPES in the millimolar range strongly inhibited the reaction. Therefore, we propose HEPES as a scaffold for

designing new P5CR inhibitors. Given that plant P5CRs share high sequence similarity, many results, obtained within the scope of this project, can be extrapolated to other plant species.

ACCESSION NUMBERS

Coordinates and structure factors of the related structures were deposited in the Protein Data Bank (PDB): *MtP5CR*-unliganded, PDB ID: 5bse; *MtP5CR*-NAD⁺ complex, 5bsf; *MtP5CR*-NADP⁺ complex, 5bsg; *MtP5CR*-Pro complex, 5bsh.

ACKNOWLEDGMENTS

This project was supported in part by the Intramural Research Program of the NCI, Center for Cancer Research. Structural results shown in this report are derived from work performed at Argonne National Laboratory, Structural Biology Center at the Advanced Photon Source. Argonne is operated by UChicago Argonne, LLC, for the U.S. Department of Energy, Office of Biological and Environmental Research under contract DE-AC02-06CH11357.

REFERENCES

- Abdelal, A. T. (1979). Arginine catabolism by microorganisms. *Annu. Rev. Microbiol.* 33, 139–168. doi: 10.1146/annurev.mi.33.100179.001035
- Altschul, S. F., Madden, T. L., Schäffer, A. A., Zhang, J., Zhang, Z., Miller, W., et al. (1997). Gapped BLAST and PSI-BLAST: a new generation of protein database search programs. *Nucleic Acids Res.* 25, 3389–3402. doi: 10.1093/nar/25.17.3389
- Armengaud, P., Thiery, L., Buhot, N., Grenier-De March, G., and Savauré, A. (2004). Transcriptional regulation of proline biosynthesis in *Medicago truncatula* reveals developmental and environmental specific features. *Physiol. Plant.* 120, 442–450. doi: 10.1111/j.0031-9317.2004.00251.x
- Britto, D. T., Ruth, T. J., Lapi, S., and Kronzucker, H. J. (2004). Cellular and whole-plant chloride dynamics in barley: insights into chloride-nitrogen interactions and salinity responses. *Planta* 218, 615–622. doi: 10.1007/s00425-003-1137-x
- Choudhary, N. L., Sairam, R. K., and Tyagi, A. (2005). Expression of δ^1 -pyrroline-5-carboxylate synthetase gene during drought in rice (*Oryza sativa* L.). *Indian J. Biochem. Biophys.* 42, 366–370.
- Coba de la Peña, T., Verdoy, D., Redondo, F. J., and Pueyo, J. J. (2003). “Salt tolerance in the Rhizobium–legume symbiosis: an overview,” in *Recent Research Developments in Plant Molecular Biology*, Vol. 1, ed S. G. Pandalai (Trivandrum: Research Signpost), 187–205.
- Csonka, L. N. (1988). Regulation of cytoplasmic proline levels in *Salmonella typhimurium*: effect of osmotic stress on synthesis, degradation, and cellular retention of proline. *J. Bacteriol.* 170, 2374–2378.
- Csonka, L. N., Gelvin, S. B., Goodner, B. W., Orser, C. S., Siemieniak, D., and Slightom, J. L. (1988). Nucleotide sequence of a mutation in the *proB* gene of *Escherichia coli* that confers proline overproduction and enhanced tolerance to osmotic stress. *Gene* 64, 199–205. doi: 10.1016/0378-1119(88)90335-6
- Csonka, L. N., and Hanson, A. D. (1991). Prokaryotic osmoregulation: genetics and physiology. *Annu. Rev. Microbiol.* 45, 569–606. doi: 10.1146/annurev.mi.45.100191.003033
- da Rocha, I. M., Vitorello, V. A., Silva, J. S., Ferreira-Silva, S. L., Viégas, R. A., Silva, E. N., et al. (2012). Exogenous ornithine is an effective precursor and the δ -ornithine amino transferase pathway contributes to proline accumulation under high N recycling in salt-stressed cashew leaves. *J. Plant Physiol.* 169, 41–49. doi: 10.1016/j.jplph.2011.08.001
- de Beer, T. A., Berka, K., Thornton, J. M., and Laskowski, R. A. (2014). PDBsum additions. *Nucleic Acids Res.* 42, D292–D296. doi: 10.1093/nar/gkt940
- Delauney, A. J., and Verma, D. P. S. (1993). Cloning of ornithine δ -aminotransferase cDNA from *Vigna aconitifolia* by trans-complementation in *Escherichia coli* and regulation of proline biosynthesis. *Plant J.* 4, 215–223. doi: 10.1046/j.1365-3113X.1993.04020215.x
- Deuschle, K., Funck, D., Forlani, G., Stransky, H., Biehl, A., Leister, D., et al. (2004). The role of δ^1 -pyrroline-5-carboxylate dehydrogenase in proline degradation. *Plant Cell* 16, 3413–3425. doi: 10.1105/tpc.104.023622
- Diederichs, K., and Karplus, P. A. (1997). Improved R-factors for diffraction data analysis in macromolecular crystallography. *Nat. Struct. Biol.* 4, 269–275. doi: 10.1038/nsb0497-269
- Emsley, P., Lohkamp, B., Scott, W. G., and Cowtan, K. (2010). Features and development of Coot. *Acta Cryst. D* 66, 486–501. doi: 10.1107/S0907444910007493
- Eschenfeldt, W. H., Makowska-Grzyska, M., Stols, L., Donnelly, M. I., Jedrzejczak, R., and Joachimiak, A. (2013). New LIC vectors for production of proteins from genes containing rare codons. *J. Struct. Funct. Genomics* 14, 135–144. doi: 10.1007/s10969-013-9163-9
- Fabro, G., Kovács, I., Pavet, V., Szabados, L., and Alvarez, M. E. (2004). Proline accumulation and *AtP5CS2* gene activation are induced by plant-pathogen incompatible interactions in *Arabidopsis*. *Mol. Plant Microbe Interact.* 17, 343–350. doi: 10.1094/MPMI.2004.17.4.343
- Forlani, G., Berlicki, L., Duò, M., Dziędziola, G., Giberti, S., Bertazzini, M., et al. (2013). Synthesis and evaluation of effective inhibitors of plant δ^1 -pyrroline-5-carboxylate reductase. *J. Agric. Food Chem.* 61, 6792–6798. doi: 10.1021/jf401234s
- Forlani, G., Bertazzini, M., Zarattini, M., Funck, D., Ruszkowski, M., and Nocek, B. (2015a). Functional properties and structural characterization of rice δ^1 -pyrroline-5-carboxylate reductase. *Front. Plant Sci.* 6:565. doi: 10.3389/fpls.2015.00565
- Forlani, G., Giberti, S., Berlicki, L., Petrollino, D., and Kafarski, P. (2007). Synthesis and evaluation of effective inhibitors of plant δ^1 -pyrroline-5-carboxylate reductase. *J. Agric. Food Chem.* 55, 4340–4347. doi: 10.1021/jf0701032
- Forlani, G., Makarova, K. S., Ruszkowski, M., Bertazzini, M., and Nocek, B. (2015b). Evolution of plant δ^1 -pyrroline-5-carboxylate reductases from phylogenetic and structural perspectives. *Front. Plant Sci.* 6:567. doi: 10.3389/fpls.2015.00567
- Forlani, G., Occhipinti, A., Berlicki, L., Dziędziola, G., Wiczorek, A., and Kafarski, P. (2008). Tailoring the structure of aminobisphosphonates to target

- plant P5C reductase. *J. Agric. Food Chem.* 56, 3193–3199. doi: 10.1021/jf800029t
- Forlani, G., Petrollino, D., Fusetti, M., Romanini, L., Nocek, B., Joachimiak, A., et al. (2012). Δ^1 -pyrroline-5-carboxylate reductase as a new target for therapeutics: inhibition of the enzyme from *Streptococcus pyogenes* and effects *in vivo*. *Amino Acids* 42, 2283–2291. doi: 10.1007/s00726-011-0970-7
- Forlani, G., Scainelli, D., and Nielsen, E. (1997). Δ^1 -pyrroline-5-carboxylate dehydrogenase from cultured cells of potato. Purification and properties. *Plant Physiol.* 113, 1413–1418.
- Funck, D., Winter, G., Baumgarten, L., and Forlani, G. (2012). Requirement of proline synthesis during *Arabidopsis* reproductive development. *BMC Plant Biol.* 12:191. doi: 10.1186/1471-2229-12-191
- Giberti, S., Funck, D., and Forlani, G. (2014). Δ^1 -Pyrroline-5-carboxylate reductase from *Arabidopsis thaliana*: stimulation or inhibition by chloride ions and feedback regulation by proline depend on whether NADPH or NADH acts as co-substrate. *New Phytol.* 202, 911–919. doi: 10.1111/nph.12701
- Haudecoeur, E., Planamente, S., Cirou, A., Tannières, M., Shelp, B. J., Moréra, S., et al. (2009). Proline antagonizes GABA-induced quenching of quorum-sensing in *Agrobacterium tumefaciens*. *Proc. Natl. Acad. Sci. U.S.A.* 106, 14587–14592. doi: 10.1073/pnas.0808005106
- Hayashi, M., Takahashi, H., Tamura, K., Huang, J., Yu, L. H., Kawai-Yamada, M., et al. (2005). Enhanced dihydroflavonol-4-reductase activity and NAD homeostasis leading to cell death tolerance in transgenic rice. *Proc. Natl. Acad. Sci. U.S.A.* 102, 7020–7025. doi: 10.1073/pnas.0502556102
- Hideg, E., Kálai, T., Hideg, K., and Vass, I. (1998). Photoinhibition of photosynthesis *in vivo* results in singlet oxygen production detection via nitroxide-induced fluorescence quenching in broad bean leaves. *Biochemistry* 37, 11405–11411. doi: 10.1021/bi972890+
- Igamberdiev, A. U., Seregélyes, C., Manac'h, N., and Hill, R. D. (2004). NADH-dependent metabolism of nitric oxide in alfalfa root cultures expressing barley hemoglobin. *Planta* 219, 95–102. doi: 10.1007/s00425-003-1192-3
- Kabsch, W. (2010). XDS. *Acta Cryst. D* 66, 125–132. doi: 10.1107/S0907444909047337
- Kabsch, W., and Sander, C. (1983). Dictionary of protein secondary structure: pattern recognition of hydrogen-bonded and geometrical features. *Biopolymers* 22, 2577–2637. doi: 10.1002/bip.360221211
- Kim, G. B., and Nam, Y. W. (2013). A novel δ^1 -pyrroline-5-carboxylate synthetase gene of *Medicago truncatula* plays a predominant role in stress-induced proline accumulation during symbiotic nitrogen fixation. *J. Plant Physiol.* 170, 291–302. doi: 10.1016/j.jplph.2012.10.004
- Kim, Y., Babnigg, G., Jedrzejczak, R., Eschenfeldt, W. H., Li, H., Maltseva, N., et al. (2011). High-throughput protein purification and quality assessment for crystallization. *Methods* 55, 12–28. doi: 10.1016/j.ymeth.2011.07.010
- Kohl, D. H., Lin, J. J., Shearer, G., and Schubert, K. R. (1990). Activities of the pentose phosphate pathway and enzymes of proline metabolism in legume root nodules. *Plant Physiol.* 94, 1258–1264. doi: 10.1104/pp.94.3.1258
- Kohl, D. H., Schubert, K. R., Carter, M. B., Hagedorn, C. H., and Shearer, G. (1988). Proline metabolism in N_2 -fixing root nodules: energy transfer and regulation of purine synthesis. *Proc. Natl. Acad. Sci. U.S.A.* 85, 2036–2040. doi: 10.1073/pnas.85.7.2036
- Kowiel, M., Jaskolski, M., and Dauter, Z. (2014). ACHESYM: an algorithm and server for standardized placement of macromolecular models in the unit cell. *Acta Cryst. D* 70, 3290–3298. doi: 10.1107/S1399004714024572
- Langer, G., Cohen, S. X., Lamzin, V. S., and Perrakis, A. (2008). Automated macromolecular model building for X-ray crystallography using ARP/wARP version 7. *Nat. Protoc.* 3, 1171–1179. doi: 10.1038/nprot.2008.91
- Lehmann, S., Funck, D., Szabados, L., and Rentsch, D. (2010). Proline metabolism and transport in plant development. *Amino Acids* 39, 949–962. doi: 10.1007/s00726-010-0525-3
- Lovell, S. C., Davis, I. W., Arendall, W. B. III., de Bakker, P. I., Word, J. M., Prisant, M. G., et al. (2003). Structure validation by $C\alpha$ geometry: ϕ , ψ and $C\beta$ deviation. *Proteins* 50, 437–450. doi: 10.1002/prot.10286
- Mattioli, R., Costantino, P., and Trovato, M. (2009). Proline accumulation in plants: not only stress. *Plant Signal. Behav.* 4, 1016–1018. doi: 10.4161/psb.4.11.9797
- Mattioli, R., Marchese, D., D'Angeli, S., Altamura, M. M., Costantino, P., and Trovato, M. (2008). Modulation of intracellular proline levels affects flowering time and inflorescence architecture in *Arabidopsis*. *Plant Mol. Biol.* 66, 277–288. doi: 10.1007/s11103-007-9269-1
- McCoy, A. J., Grosse-Kunstleve, R. W., Adams, P. D., Winn, M. D., Storoni, L. C., and Read, R. J. (2007). Phaser crystallographic software. *J. Appl. Crystallogr.* 40, 658–674. doi: 10.1107/S0021889807021206
- Meng, Z., Lou, Z., Liu, Z., Li, M., Zhao, X., Bartlam, M., et al. (2006). Crystal structure of human pyrroline-5-carboxylate reductase. *J. Mol. Biol.* 359, 1364–1377. doi: 10.1016/j.jmb.2006.04.053
- Merrill, M. J., Yeh, G. C., and Phang, J. M. (1989). Purified human erythrocyte pyrroline-5-carboxylate reductase. Preferential oxidation of NADPH. *J. Biol. Chem.* 264, 9352–9358.
- Minor, W., Cymborowski, M., Otwinowski, Z., and Chruszcz, M. (2006). HKL-3000: the integration of data reduction and structure solution—from diffraction images to an initial model in minutes. *Acta Cryst. D* 62, 859–866. doi: 10.1107/S0907444906019949
- Murahama, M., Yoshida, T., Hayashi, F., Ichino, T., Sanada, Y., and Wada, K. (2001). Purification and characterization of δ^1 -pyrroline-5-carboxylate reductase isoenzymes, indicating differential distribution in spinach (*Spinacia oleracea* L.) leaves. *Plant Cell Physiol.* 42, 742–750. doi: 10.1093/pcp/pc093
- Murshudov, G. N., Skubák, P., Lebedev, A. A., Pannu, N. S., Steiner, R. A., Nicholls, R. A., et al. (2011). REFMAC5 for the refinement of macromolecular crystal structures. *Acta Cryst. D* 67, 355–367. doi: 10.1107/S0907444911001314
- Nicholls, R. A., Fischer, M., McNicholas, S., and Murshudov, G. N. (2014). Conformation-independent structural comparison of macromolecules with ProSMART. *Acta Cryst. D* 70, 2487–2499. doi: 10.1107/S1399004714016241
- Nocek, B., Chang, C., Li, H., Lezondra, L., Holzle, D., Collart, F., et al. (2005). Crystal structures of δ^1 -pyrroline-5-carboxylate reductase from human pathogens *Neisseria meningitidis* and *Streptococcus pyogenes*. *J. Mol. Biol.* 354, 91–106. doi: 10.1016/j.jmb.2005.08.036
- Petrollino, D., and Forlani, G. (2012). Coenzyme preference of *Streptococcus pyogenes* δ^1 -pyrroline-5-carboxylate reductase: evidence supporting NADPH as the physiological electron donor. *Amino Acids* 43, 493–497. doi: 10.1007/s00726-011-1077-x
- Pettersen, E. F., Goddard, T. D., Huang, C. C., Couch, G. S., Greenblatt, D. M., Meng, E. C., et al. (2004). UCSF Chimera—a visualization system for exploratory research and analysis. *J. Comput. Chem.* 25, 1605–1612. doi: 10.1002/jcc.20084
- Rayapati, P. J., Stewart, C. R., and Hack, E. (1989). Pyrroline-5-carboxylate reductase is in pea (*Pisum sativum* L.) leaf chloroplasts. *Plant Physiol.* 91, 581–586. doi: 10.1104/pp.91.2.581
- Rosenbaum, G., Alkire, R. W., Evans, G., Rotella, F. J., Lazarski, K., Zhang, R. G., et al. (2006). The Structural Biology Center 191D undulator beamline: facility specifications and protein crystallographic results. *J. Synchrotron Radiat.* 13, 30–45. doi: 10.1107/S0909049505036721
- Saradhi, P. P., Alia Arora, S., and Prasad, K. V. (1995). Proline accumulates in plants exposed to UV radiation and protects them against UV induced peroxidation. *Biochem. Biophys. Res. Commun.* 209, 1–5. doi: 10.1006/bbrc.1995.1461
- Schat, H., Sharma, S. S., and Vooijs, R. (1997). Heavy metal-induced accumulation of free proline in a metal-tolerant and a nontolerant ecotype of *Silene vulgaris*. *Physiol. Plant.* 101, 477–482. doi: 10.1111/j.1399-3054.1997.tb01026.x
- Smith, R. J., Downing, S. J., Phang, J. M., Lodato, R. F., and Aoki, T. T. (1980). Pyrroline-5-carboxylate synthase activity in mammalian cells. *Proc. Natl. Acad. Sci. U.S.A.* 77, 5221–5225. doi: 10.1073/pnas.77.9.5221
- Szabados, L., and Savouré, A. (2010). Proline: a multifunctional amino acid. *Trends Plant Sci.* 15, 89–97. doi: 10.1016/j.tplants.2009.11.009
- Székely, G., Abrahám, E., Csépló, A., Rigó, G., Zsigmond, L., Csiszár, J., et al. (2008). Duplicated P5CS genes of *Arabidopsis* play distinct roles in stress regulation and developmental control of proline biosynthesis. *Plant J.* 53, 11–28. doi: 10.1111/j.1365-313X.2007.03318.x
- Szoke, A., Miao, G. H., Hong, Z., and Verma, D. P. (1992). Subcellular location of δ^1 -pyrroline-5-carboxylate reductase in root/nodule and leaf of soybean. *Plant Physiol.* 99, 1642–1649. doi: 10.1104/pp.99.4.1642
- Takahashi, H., Takahara, K., Hashida, S. N., Hirabayashi, T., Fujimori, T., Kawai-Yamada, M., et al. (2009). Pleiotropic modulation of carbon and nitrogen metabolism in *Arabidopsis* plants overexpressing the *NAD kinase2* gene. *Plant Physiol.* 151, 100–113. doi: 10.1104/pp.109.140665

- Trinchant, J. C., Yang, Y. S., and Rigaud, J. (1998). Proline accumulation inside symbiosomes of faba-bean nodules under salt stress. *Physiol. Plant.* 104, 38–49. doi: 10.1034/j.1399-3054.1998.1040106.x
- UniProt Consortium. (2015). UniProt: a hub for protein information. *Nucleic Acids Res.* 43, D204–D212. doi: 10.1093/nar/gku989
- Verdoy, D., Coba De La Peña, T., Redondo, F. J., Lucas, M. M., and Pueyo, J. J. (2006). Transgenic *Medicago truncatula* plants that accumulate proline display nitrogen-fixing activity with enhanced tolerance to osmotic stress. *Plant Cell Environ.* 29, 1913–1923. doi: 10.1111/j.1365-3040.2006.01567.x
- Verslues, P. E., and Sharma, S. (2010). Proline metabolism and its implications for plant-environment interaction. *Arabidopsis Book* 8:e0140. doi: 10.1199/tab.0140
- Williams, I., and Frank, L. (1975). Improved chemical synthesis and enzymatic assay of δ^1 -pyrroline-5-carboxylic acid. *Anal. Biochem.* 64, 85–97. doi: 10.1016/0003-2697(75)90408-X
- Winn, M. D., Isupov, M. N., and Murshudov, G. N. (2001). Use of TLS parameters to model anisotropic displacements in macromolecular refinement. *Acta Cryst. D* 57, 122–133. doi: 10.1107/S0907444900014736
- Winter, G., Todd, C. D., Trovato, M., Forlani, G., and Funck, D. (2015). Physiological implications of arginine metabolism in plants. *Front. Plant Sci.* 6:534. doi: 10.3389/fpls.2015.00534
- Yang, S. L., Lan, S. S., and Gong, M. (2009). Hydrogen peroxide-induced proline and metabolic pathway of its accumulation in maize seedlings. *J. Plant Physiol.* 166, 1694–1699. doi: 10.1016/j.jplph.2009.04.006
- Yoshida, Y., Kiyosue, T., Katagiri, T., Ueda, H., Mizoguchi, T., Yamaguchi-Shinozaki, K., et al. (1995). Correlation between the induction of a gene for δ^1 -pyrroline-5-carboxylate synthetase and the accumulation of proline in *Arabidopsis thaliana* under osmotic stress. *Plant J.* 7, 751–760. doi: 10.1046/j.1365-313X.1995.07050751.x

Conflict of Interest Statement: The authors declare that the research was conducted in the absence of any commercial or financial relationships that could be construed as a potential conflict of interest.

Copyright © 2015 Ruszkowski, Nocek, Forlani and Dauter. This is an open-access article distributed under the terms of the Creative Commons Attribution License (CC BY). The use, distribution or reproduction in other forums is permitted, provided the original author(s) or licensor are credited and that the original publication in this journal is cited, in accordance with accepted academic practice. No use, distribution or reproduction is permitted which does not comply with these terms.